Statistical data for the tensile properties and static fatigue of sic-based bundles

S. Mazerat, R. Pailler

Article Title

Statistical data for the tensile properties and static fatigue of SiC-based bundles

Authors

S. Mazerat, R. Pailler*

Affiliations

Univ. Bordeaux, CNRS, CEA, SAFRAN CERAMICS, LCTS, UMR 5801, F-33600 Pessac, France

Corresponding author

René Pailler

E-Mail: pailler@lcts.u-bordeaux.fr

Tel: +33 5 56 84 47 33

Abstract

Due to their high specific strength at elevated temperatures and resistance to oxidative environments, SiC-based fibers are of great interest for the reinforcement of ceramic matrix composites. They are however subjected to a slow crack growth (SCG) phenomenon causing their delayed failure under subcritical conditions. The testing of filaments, other than comprising handling difficulties, requires large sets of data (broadly dispersed), drawback alleviated by multifilament tow testing. The data available in the present paper correspond to a comprehensive mechanical characterization and static fatigue testing of various types of SiC-based fiber bundles. The initial non-linearity of load displacement curves were analyzed to reveal the tow structure originating from filament misalignment. Static fatigue tests were used to assess the lifetime prediction coefficients and its distribution parameters. These data may found interest for the interpretation of dispersion bundle testing can highlight under different solicitation mode. Such data are also prominent for the wealth of composite design and to guaranty long term performances over the broad application field offered.

Keywords

Bundle tensile testing ; Filament load distribution ; Fiber slack ; Slow crack growth ; Delayed failure ; Static fatigue

Specifications Table

Subject	Material Science
Specific subject area	Tensile testing and static fatigue of SiC-based bundle
Type of data	Table Figure
How data were acquired	Tensile and static fatigue were assessed on bundle samples using the same probe preparation method. The bundle structure parameters were deduced from force displacement curves, while the lifetimes were acquire suspending a dead weight to a bundle placed in a resistive furnace opened to ambient atmosphere, and measuring the time before its failure.
Data format	Raw and analyzed
Parameters for data collection	Different fiber bundle types (Nicalon or Tyranno) were repeatedly tested. Batch to batch variability was observed on NL207, fiber diameter on Grade S, effect of desizing and chlorination surface treatment on ZMI. Tensile tests were performed at a unique strain rate. Static fatigue tests were performed at different stresses (300-1500 MPa) or temperatures (350-900 °C).
Description of data collection	Force displacement curve were analyzed to extract the tensile strength and structure. This latter factor is related to fiber misalignment. The time separating the testing startup and the bundle failure defined the lifetime. Statistical parameters describing the variability of these data were assessed by linear regression of Weibull plots.
Data source location	Univ. Bordeaux, CNRS, CEA, SAFRAN CERAMICS, LCTS, UMR 5801, F-33600 Pessac, France
Data accessibility	With the article

Value of the Data

- This dataset is valued because it comprises significant amount of bundle strength and time to failure data to assess dispersion parameters. The fiber slack is also revealed.
- The data presented herein may be used to assist the analysis of trials performed on multifilament tows, such as tensile or fatigue.
- The presented data can assist the selection of a reinforcement type for a given application (design on purpose), based on bundle mechanical properties and

predicted lifetime. It may also be used to interpret bundle testing, with emphasis on the filament misalignment.

- These data show how the strength, effective section (γ) and standard deviation on filament load (here called ς), can be fitted by a Weibull type distribution law.
- These data would help to understand how the composition or microstructural parameters influence the delayed failure. This may be further used for future fiber development.

1. Data Description

This data article presents series of mechanical characterizations for 8 types of SiC-based fiber bundle (Nicalon NL101, Nicalon NL207, Hi-Nicalon, Hi-Nicalon Type S, Tyranno Grade S, Tyranno Lox-M, Tyranno ZMI and Tyranno AM) repeatedly performed for statistical parameters assessment (Weibull distribution law). This number was brought to 11 and 12 respectively at single filament and multifilament tow testing scales, including different batches or surface treatments [1,2]. Fibers chemical composition and microstructure were presented in Ref. [3]. Filaments cover a broad range of mean tensile strength extending form 2000 to 4000 MPa, with Weibull moduli in the 5-10 range (Table 1). The Young modulus for these fibers reflects their microstructure, lying about 200 GPa for the SiCO first generation, and above for oxygen free second or third generations (respectively Hi-Nicalon and Hi-Nicalon S). On ZMI fibers the surface transformation by chlorination treatment had a markedly beneficial effect on tensile strength (4000 vs. 3000 MPa) and Weibull modulus (10 vs. 5). This was interpreted by depletion of severest surface located defects [1].

Bundle tensile testing comprises more complexity due to fact several hundred of filaments are simultaneously loaded. Their ruin is indeed characterized by a damage tolerant behavior (Fig. 1), resulting from progressive filament breaks and load sharing. The individual bundle tensile strengths are gathered in tables 2-4 and summarized in Table 5. With mean strengths extending from 750 MPa to 1800 MPa and Weibull moduli from 4 to 30 (Fig. 2, Table 5), these data did not followed the filament strength ranking. NL207, NL101, ZMI_{Cl} and AM tows, all standing below 900 MPa, covered the full above mentioned filament strength range. Despite no measured difference between sized or unsized ZMI filament strengths, tows made with the latter were weaker. The same phenomenon may explain fact the beneficial effect of chlorination treatment was lost at bundle scale.

These discrepancies can be explained by filament misalignment, characterized by the 2 following parameters: (i). γ, proportion of unloaded fiber (Eq. (3), considered for bundle strength calculation) and (ii). δ_F, filament load distribution with ς as standard deviation (Eq. (5)). This latter is revealed by the progressive initial loading stage (Fig 3 Eq. (4)), early loaded fibers ending up being overloaded and vice versa (Fig. 4). These structural parameters were

assessed for each test, presented in Tables 2-4, and were ascribed a Weibull statistical distribution (Figs 5-16, Table 6). The relevance of these statistical laws (Eqs. (6) and (7)) was evaluated with the Kolmogorov–Smirnov test, comparing empirical and predicted distributions. It was revealed that the percentile accurately reflected the Weibull model on ς and γ at a significance level standing below the respective D_α ($D_{\alpha\,(30)}$ = 0.24 for instance).

A broad range of tow structures were evidenced, going from very limited slack observed in Tyranno Grade S (named TS) to high misalignment illustrated by Hi-Nicalon S (Hi-Ni-S). This work points out the batch to batch (NL207) but also probe to probe structure difference one should be aware of when testing bundle specimen. These are strongly method related, large discrepancies being therefore expected comparing different testing approaches (gauge length, grip gluing…). Moreover, despite fact one single ZMI batch was used for this work, sizing removal led to a drastic increase of γ ($ZMI^{\ddagger}$ and ZMI_{Cl}), explained by sample preparation difficulties.

To complete this work, static fatigue testing were performed on the same samples to determine the lifetime prediction parameters for the different fiber types above mentioned. Two different testing approaches were followed. The first aimed at lifetime distribution assessment (Fig. 17, Tables 7 and 8) whereas the second one focused on discrete stress scanning (Fig. 18) for lifetime prediction parameters estimation (Fig. 19, Table 9), following an empirical power law ($t = A\sigma^{-n}$, with t the lifetime, σ the applied stress, A and n material constants). Lifetime Weibull moduli ranging from 0.5 to 2 were assessed. Globally, sized Tyranno® fiber types display a lower dispersion, characterized by higher Weibull moduli, than Nicalon. This observation is coherent with their strength distribution (Table 5). The consistency of this lifetime modulus for different testing conditions (stress or temperature) should be emphases.

The engineering stress correction (Eq. (1)) convincingly compensated the batch to batch variability as shown in Fig. 18a. No particular evolution of stress exponents with temperature is to be noted, thus these values were averaged to define this intrinsic value. For here reported fiber types, this parameter extended from 5 to 9, Lox-M and ZMI being respectively the lower and upper limits. Despite displaying clear different microstructure, Hi-Nicalon and Hi-Nicalon S did not showed particular behavior. It was demonstrated the coefficient A

follows an Arrhenius type law, presented in figure 19 for NL207, Grade S, Lox-M and ZMI fibers with apparent activation energies lying in the 100-200 kJ mol^{-1} range. It is worth noting values for A extracted at T>650°C for Tyranno® fibers did not followed the global trend. Some of the Weibull plots presented in this work were not perfectly aligned, incoherence that could be ascribed to sample preparation (selection of the probe) and to the limited number of tests.

Fiber	Density ($g\ cm^{-3}$)	$\sigma_{f.f}$ ± std. dev. (MPa)	E_f (GPa)	m_f	$\sigma_{1.f}$ (MPa)	K_{IC} (MPa $m^{1/2}$)	Compliance (µm N^{-1})
NL101	2.57	2166 ± 559	180	4.28	2390	1.20	48
NL207	2.58	2839 ± 667	210	5.05	3090	1.20	43
NL207*	2.58	2672 ± 710	210	4.35	2950	1.20	20
Hi-Ni	2.74	3136 ± 368	300	9.84	3295	1.66	24
Hi-Ni-S	3.05	2877 ± 414	410	8.42	3062	1.86	110
TS	2.35	3152 ± 624	180	8.17	3550	1.11	180
TS11	2.35	2776 ± 647	180	4.79	3034	1.12	170
Lox-M	2.37	2984 ± 695	200	4.63	3314	1.11	86
ZMI	2.48	3076 ± 742	200	4.81	3372	1.01	150
ZMI_{Cl}	2.48	4039 ± 479	220	9.99	4265	1.01	115
AM	2.42	2815 ± 533	180	5.74	3024	1.20	84

Table 1: Physical and mechanical properties of filaments. Sized and unsized ZMI filaments are not differentiated.

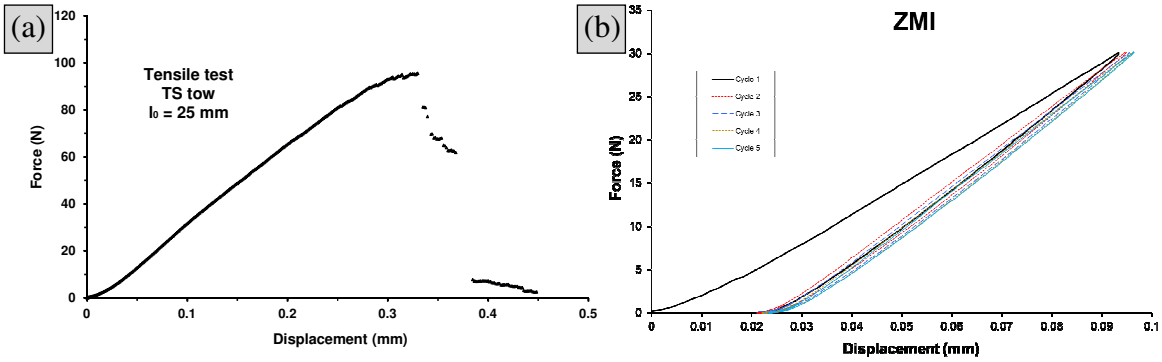

Fig. 1: Load displacement curve for (a). TS bundle tensile test highlighting the damage tolerant failure mode and (b). cycling in 0-30 N range on a ZMI tow.

Hi-Ni			Hi-Ni-S			NL207		
γ	$\sigma_{f.f(\gamma)}$	ς	γ	$\sigma_{f.f(\gamma)}$	ς	γ	$\sigma_{f.f(\gamma)}$	ς
0.029	2125	0.0183	0.534	1665	0.0740	0.076	790	0.0173
0.081	1955	0.0231	0.363	1448	0.0569	0.058	724	0.0252
0.195	1323	0.0251	0.381	1148	0.0589	0.230	616	0.0225
0.115	2147	0.0289	0.507	1306	0.0561	0.035	738	0.0249
0.082	2042	0.0223	0.438	1422	0.0517	0.151	712	0.0361
-0.050	1826	0.0189	0.411	1581	0.0404	0.069	762	0.0204
0.133	1967	0.0317	0.137	1854	0.0304	0.171	766	0.0246
0.172	1767	0.0305	0.187	1572	0.0154	-0.023	605	0.0254
0.172	1767	0.0305	0.228	1645	0.0258	0.245	643	0.0225
0.396	1907	0.0345	0.196	1612	0.0461	0.061	697	0.0297
0.254	1910	0.0287	0.146	1712	0.0522	0.200	859	0.0249
-0.001	1142	0.0191	0.075	1650	0.0323	0.000	798	0.0257
0.274	1986	0.0284	0.239	1685	0.0423	-0.011	860	0.0236
0.149	1937	0.0261	0.149	1668	0.0326	0.128	680	0.0267
0.123	1965	0.0242	0.041	1681	0.0282	0.216	585	0.0265
0.302	1843	0.0241	0.465	1621	0.0394	0.135	661	0.0271
-0.014	1418	0.0244	0.013	1872	0.0226	0.059	549	0.0257
0.370	1953	0.0288	0.243	1445	0.0344	0.102	929	0.0192
0.220	1751	0.0326	0.058	1799	0.0338	-0.055	946	0.0217
0.001	2039	0.0271	0.060	1827	0.0281	0.146	636	0.0260
0.177	1852	0.0271	0.341	1469	0.0408	0.264	1019	0.0255
0.099	1936	0.0256	0.429	2039	0.0610	0.201	816	0.0232
0.115	1774	0.0258	0.171	2039	0.0418	0.159	905	0.0201
-0.007	1889	0.0193	0.472	1259	0.0441	0.138	879	0.0251
0.173	1280	0.0253	0.173	1727	0.0371	0.119	858	0.0246
0.143	1848	0.0297	0.182	1811	0.0297	0.295	675	0.0260
0.271	2130	0.0275				-0.110	857	0.0291
0.170	1738	0.0294				0.019	644	0.0241
0.090	1679	0.0183				-0.008	753	0.0248
-0.003	1977	0.0223				0.042	713	0.0274

Table 2: Raw data for the tensile behavior of Hi-Ni, Hi-Ni-S and NL207 bundles.

TS11			Lox-M			ZMI		
γ	$\sigma_{f.f(\gamma)}$	ς	γ	$\sigma_{f.f(\gamma)}$	ς	γ	$\sigma_{f.f(\gamma)}$	ς
0.170	1124	0.0258	0.220	1378	0.0185	0.125	1347	0.0162
0.131	1161	0.0203	0.220	1353	0.0199	0.034	1311	0.0165
0.185	1177	0.0179	0.246	1339	0.0197	0.226	1299	0.0284
0.221	1112	0.0257	0.331	1205	0.0233	0.165	1396	0.0255
0.145	1135	0.0155	0.125	1435	0.0172	0.261	1136	0.0213
0.033	1244	0.0145	0.270	1435	0.0222	0.201	1294	0.0198
0.018	1228	0.0129	0.222	1347	0.0176	0.110	1403	0.0176
0.178	838	0.0182	0.202	1405	0.0212	0.279	1230	0.0158
0.091	1202	0.0206	0.386	1387	0.0219	0.203	1329	0.0173
0.183	1050	0.0187	0.261	1429	0.0269	0.190	1329	0.0270
0.072	1127	0.0176	0.371	1439	0.0216	0.125	1350	0.0304
0.051	1133	0.0134	0.201	1294	0.0279	0.048	1371	0.0169
0.144	1167	0.0160	0.170	1385	0.0302	0.152	1396	0.0214
0.012	1261	0.0143	0.375	1496	0.0228	-0.012	1361	0.0145
0.015	1140	0.0174	0.209	1357	0.0227	0.073	1358	0.0240
0.035	1216	0.0203	0.174	1389	0.0337	0.129	1317	0.0293
0.152	1063	0.0222	0.205	1348	0.0262	0.045	1304	0.0156
0.023	1267	0.0113	0.314	1341	0.0324	0.033	1333	0.0215
0.331	1022	0.0235	0.368	1431	0.0235	0.255	1329	0.0263
0.115	1067	0.0192	0.179	1315	0.0346	0.145	1519	0.0244
0.030	1199	0.0188	0.385	1444	0.0284	0.147	1421	0.0203
0.108	1174	0.0174	0.255	1391	0.0224	0.073	1431	0.0215
0.050	1182	0.0181	0.339	1426	0.0219	0.015	1387	0.0171
0.040	1138	0.0135	0.143	1425	0.0174	0.117	1431	0.0167
0.172	1159	0.0229	0.143	1425	0.0166	0.235	1429	0.0272
0.224	1137	0.0175	0.350	1505	0.0205	0.226	1439	0.0261
0.020	1169	0.0169	0.217	1392	0.0245	0.204	1352	0.0201
0.110	1103	0.0143	0.218	1367	0.0294	0.138	1405	0.0199
0.106	1113	0.0161	0.204	1390	0.0268	-0.035	1366	0.0140
0.058	1002	0.0146	0.338	1428	0.0288	0.185	1341	0.0191

Table 3: Raw data for the tensile behavior of TS11, Lox-M and ZMI bundles.

Nl207*			ZMI‡			ZMI_{Cl}		
γ	$\sigma_{f.f(\gamma)}$	ς	γ	$\sigma_{f.f(\gamma)}$	ς	γ	$\sigma_{f.f(\gamma)}$	ς
0.097	878	0.0324	0.392	912	0.0247	0.205	686	0.0145
0.256	890	0.0261	0.170	873	0.0129	0.237	537	0.0119
0.181	1055	0.0233	0.305	1112	0.0183	0.277	679	0.0186
0.146	990	0.0241	0.297	928	0.0150	0.154	570	0.0117
0.117	897	0.0224	0.187	1061	0.0150	0.474	1146	0.0205
0.150	972	0.0332	0.148	770	0.0206	0.368	1006	0.0180
0.199	794	0.0273	0.256	950	0.0221	0.289	1208	0.0182
0.232	841	0.0257	0.279	980	0.0235	0.249	662	0.0199
0.138	1070	0.0278	0.261	1072	0.0238	0.287	772	0.0181
0.321	934	0.0255	0.375	882	0.0211	0.320	674	0.0185
0.256	979	0.0358	0.303	973	0.0287	0.323	604	0.0194
0.278	1182	0.0205	0.283	1075	0.0234	0.240	978	0.0173
0.172	918	0.0253	0.232	890	0.0136	0.251	580	0.0170
0.352	908	0.0201	0.300	959	0.0295	0.189	948	0.0149
0.231	973	0.0296	0.176	819	0.0142	0.257	692	0.0174
0.199	701	0.0242	0.161	759	0.0207	0.210	622	0.0159
0.179	926	0.0184	0.165	971	0.0149	0.299	731	0.0192
0.171	741	0.0334	0.201	818	0.0178			
0.198	969	0.0225	0.225	840	0.0191			
0.191	996	0.0278	0.173	954	0.0166			
0.207	928	0.0286	0.276	1275	0.0165			
0.198	650	0.0289	0.296	1145	0.0185			
0.154	799	0.0254	0.233	1186	0.0181			
0.202	828	0.0384	0.357	995	0.0199			
0.141	692	0.0258	0.293	1213	0.0231			
0.184	816	0.0309	0.290	910	0.0175			
0.080	819	0.0227	0.297	1000	0.0209			
0.157	683	0.0270	0.260	729	0.0181			
0.151	688	0.0203	0.322	1102	0.0200			
0.302	652	0.0296	0.225	788	0.0247			

Table 4: Raw data for the tensile behavior of NL207*, ZMI‡ and ZMI_{Cl} bundles.

	Number of tests	$\sigma_{f,t(\bar{\gamma})}$ (MPa)	$F_{f,t}$ (N)	m_t	$\sigma_{0.t}$ (MPa)	Compliance (µm N^{-1})
NL101	30	870	57	4.8	940	1.6
NL207	30	750	57	7.8	810	1.4
NL207*	30	870	60	7.8	928	0.60
Hi-Ni	30	1800	120	7.9	1930	1.6
Hi-Ni-S	26	1600	82	9.0	1730	1.3
TS	100	1300	100	17	1380	0.90
TS11	30	1100	87	15	1180	1.6
Lox-M	30	1400	95	28	1420	0.80
ZMI	30	1350	110	23	1390	1.2
ZMI‡	28	960	57	8.1	1020	0.68
ZMI_{Cl}	18	770	37	4.4	840	1.3
AM	30	810	60	6.2	870	1.1

Table 5: Mechanical properties of SiC-based multifilament tows.

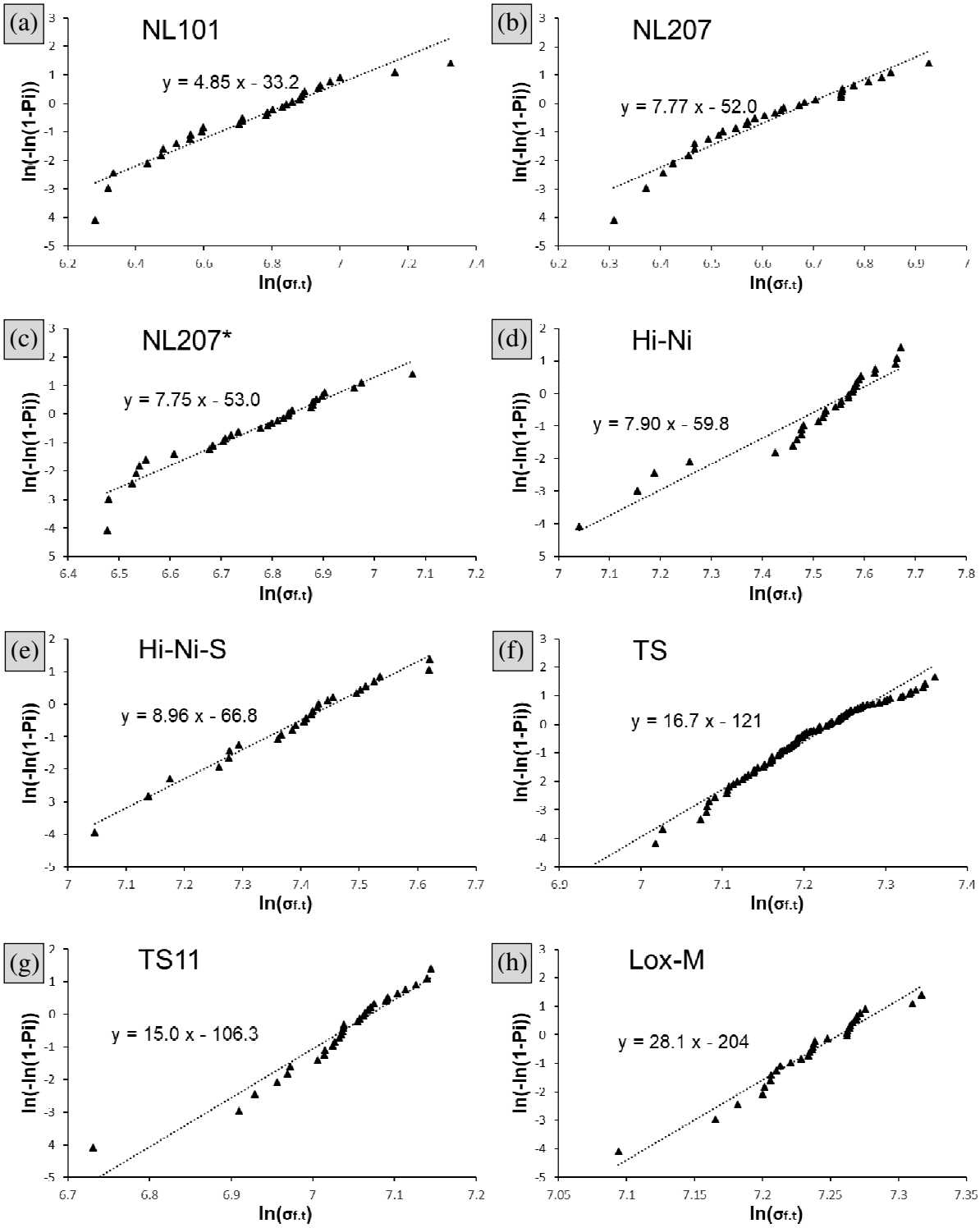
(a)
NL101
y = 4.85 x - 33.2
(b)
NL207
y = 7.77 x - 52.0
(c)
NL207*
y = 7.75 x - 53.0
(d)
Hi-Ni
y = 7.90 x - 59.8
(e)
Hi-Ni-S
y = 8.96 x - 66.8
(f)
TS
y = 16.7 x - 121
(g)
TS11
y = 15.0 x - 106.3
(h)
Lox-M
y = 28.1 x - 204
ln(-ln(1-Pi))
ln(σf.t)

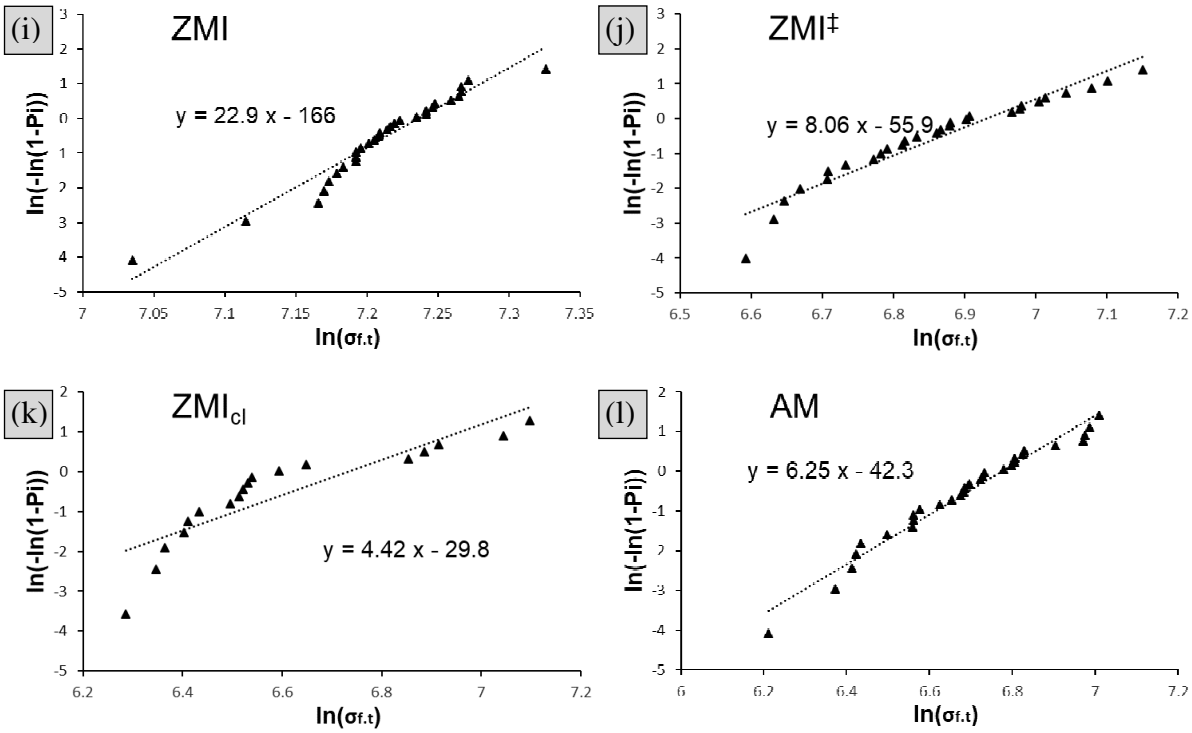

Fig. 2: Weibull plots for bundle tensile strength of (a). Nicalon NL101 (b). Nicalon NL207 (c). Nicalon NL207* (second batch) (d). Hi-Nicalon (e). Hi-Nicalon Type S (f). Tyranno Grade S 8.5 µm mean diameter (g). Tyranno Grade S 11 µm mean diameter (h). Tyranno Lox-M (i). Tyranno ZMI (j). Tyranno ZMI‡ (desized) (k). Tyranno ZMI_{Cl} (chlorinated) (l). Tyranno AM.

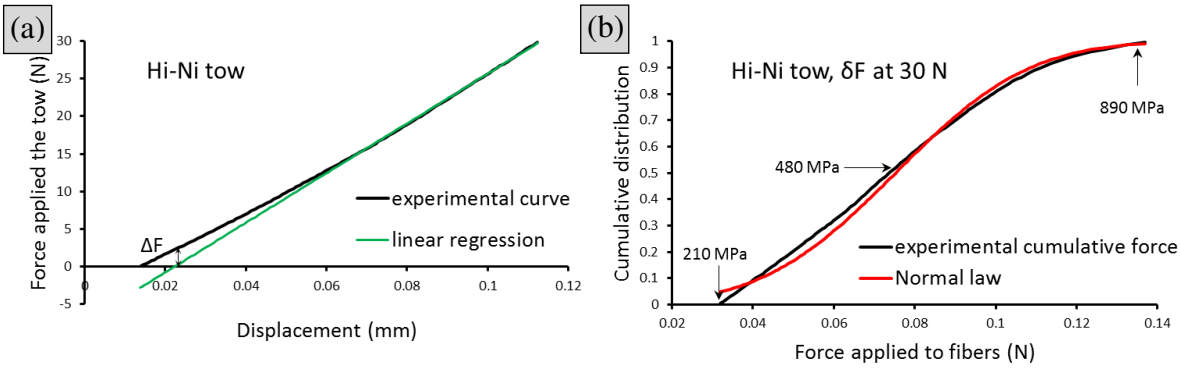

Fig. 3: (a). Initial loading of a Hi-Ni tow (0-30 N range), used to estimate the load distribution (b). derived from deviation to linearity. On this example, ς = 0.026 N, $\overline{w}_f$ = 0.075 N and γ = 22%.

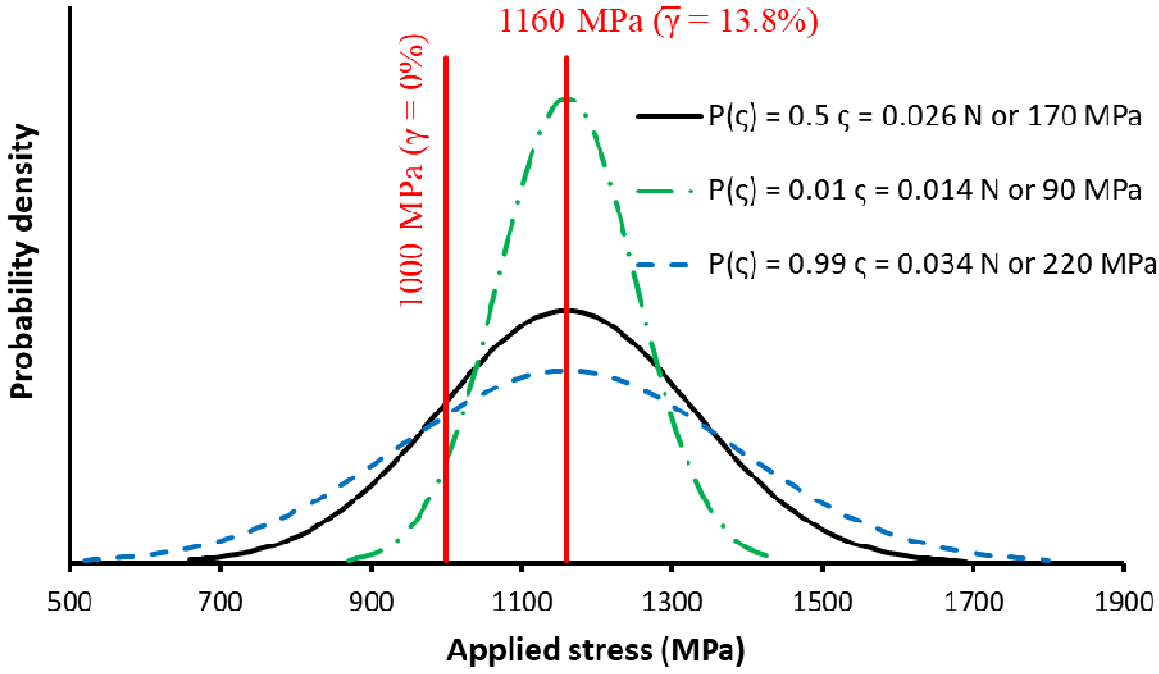

Fig. 4: Distribution of stress applied to Hi-Ni fibers considering the structural aspects: effective section ($\bar{\gamma}$) and fiber slacking with 3 different standard deviations (ς) corresponding to a probability of 0.01, 0.5 and 0.99 on the Weibull distribution (Eq. (6)).

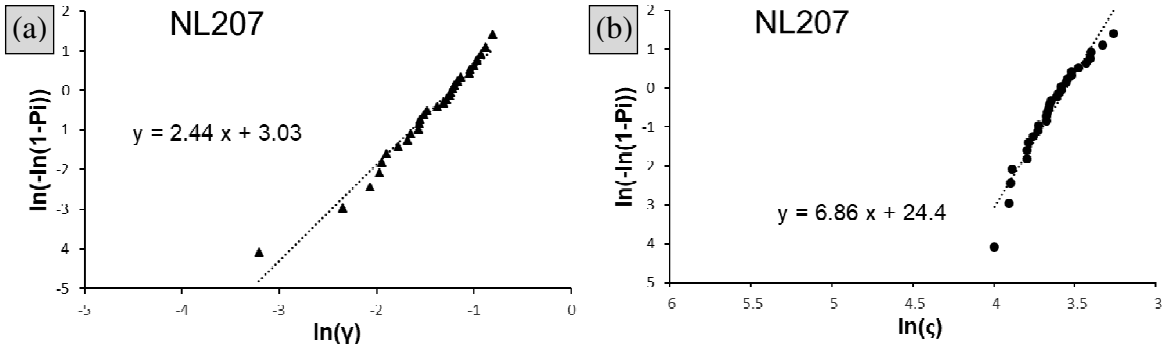

Fig. 5: Weibull representation of structural parameters (a). γ (effective section fraction with a 15% offset) and (b). ς (standard deviation of fiber load distribution) on Nicalon NL207 fiber tows.

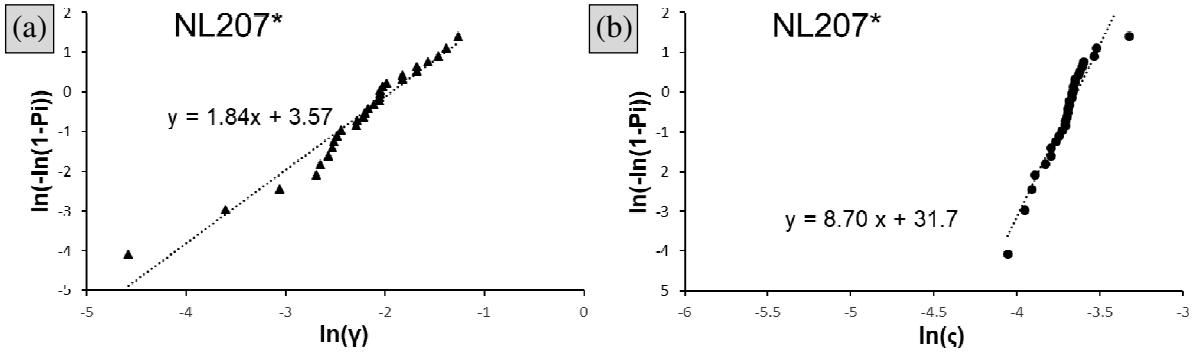

Fig. 6: Weibull representation of structural parameters (a). γ (effective section fraction with a -7% offset) and (b). ς (standard deviation of fiber load distribution) on Nicalon NL207* fiber tows.

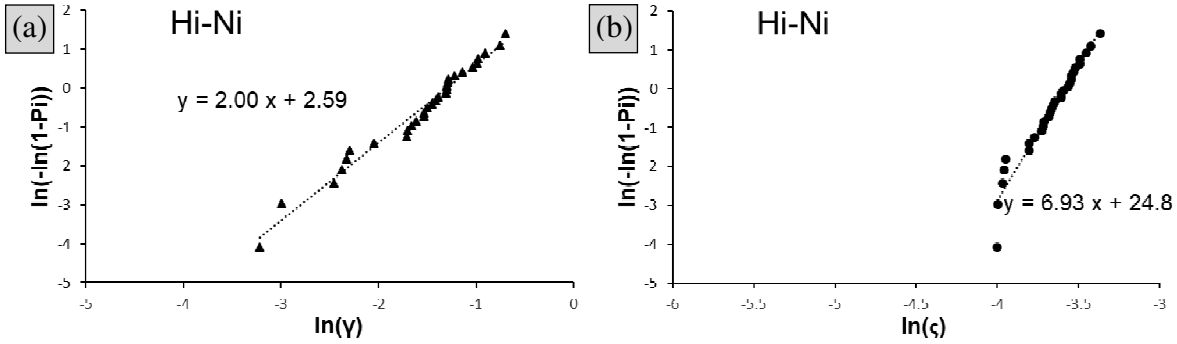

Fig. 7: Weibull representation of structural parameters (a). γ (effective section fraction with a 10% offset) and (b). ς (standard deviation of fiber load distribution) on Hi-Nicalon fiber tows.

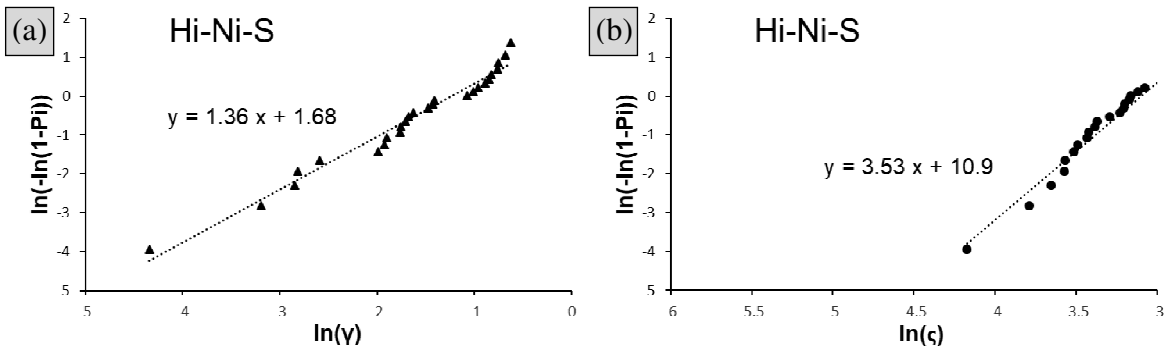

Fig. 8: Weibull representation of structural parameters (a). γ (effective section fraction) and (b). ς (standard deviation of fiber load distribution) on Hi-Nicalon Type S fiber tows.

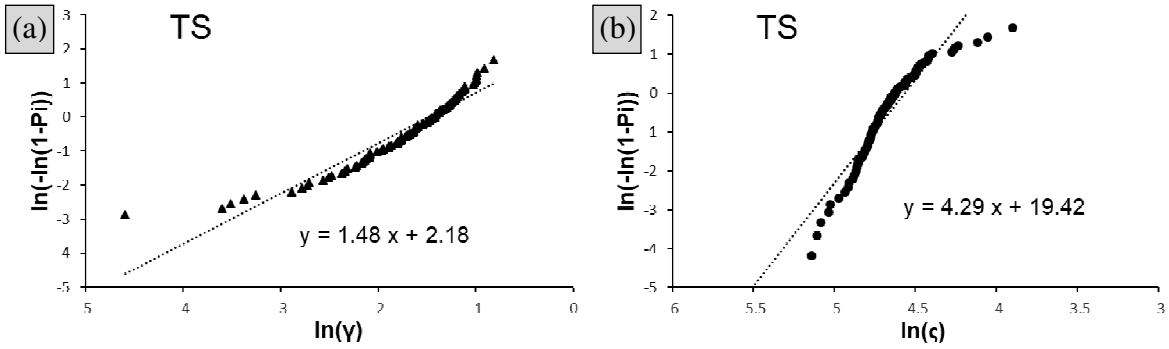

Fig. 9: Weibull representation of structural parameters (a). γ (effective section fraction) and (b). ς (standard deviation of fiber load distribution) on Tyranno Grade S (8.5 µm diameter, TS) fiber tows.

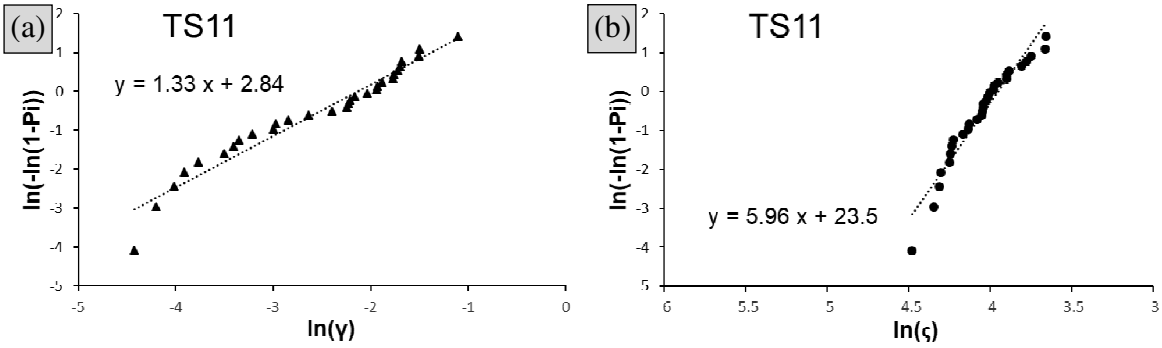

Fig. 10: Weibull representation of structural parameters (a). γ (effective section fraction) and (b). ς (standard deviation of fiber load distribution) on Tyranno Grade S (11 µm diameter, TS11) fiber tows.

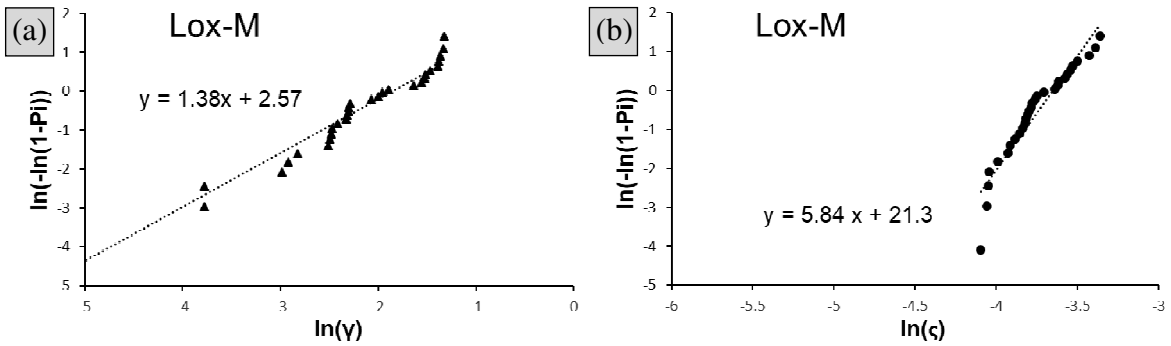

Fig. 11: Weibull representation of structural parameters (a). γ (effective section fraction with a -12% offset) and (b). ς (standard deviation of fiber load distribution) on Tyranno Lox-M fiber tows.

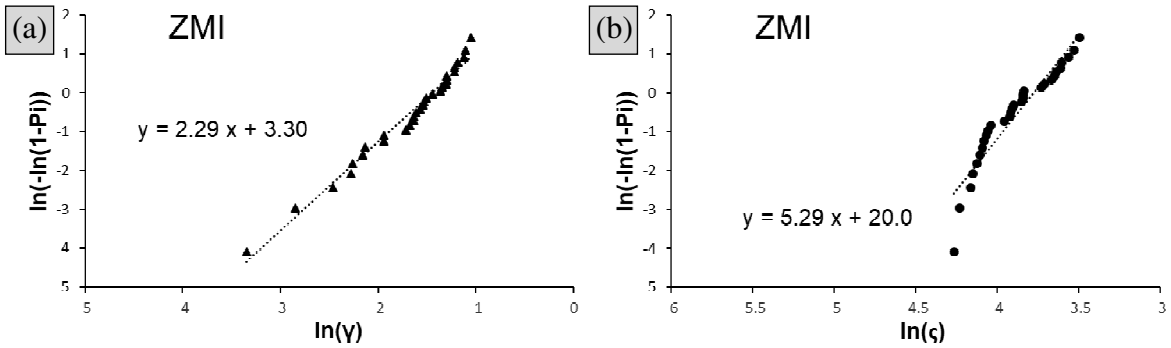

Fig. 12: Weibull representation of structural parameters (a). γ (effective section fraction with a 7% offset) and (b). ς (standard deviation of fiber load distribution) on Tyranno ZMI fiber tows.

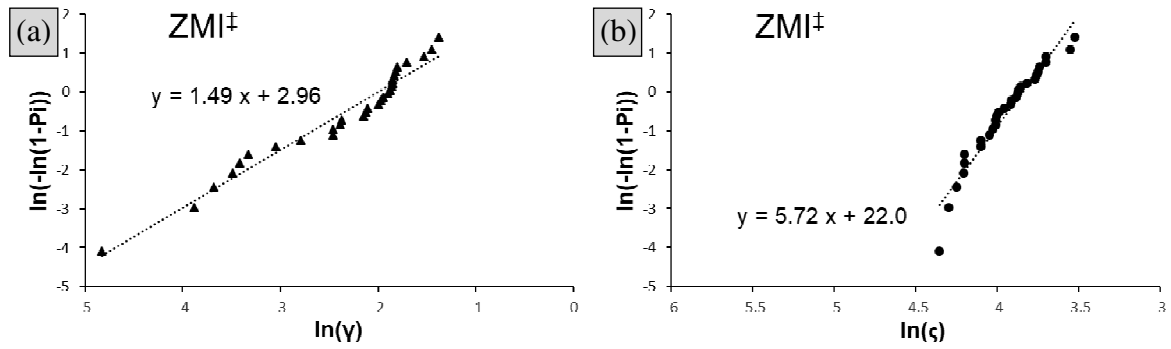

Fig. 13: Weibull representation of structural parameters (a). γ (effective section fraction with a -14% offset) and (b). ς (standard deviation of fiber load distribution) on unsized Tyranno ZMI fiber tows.

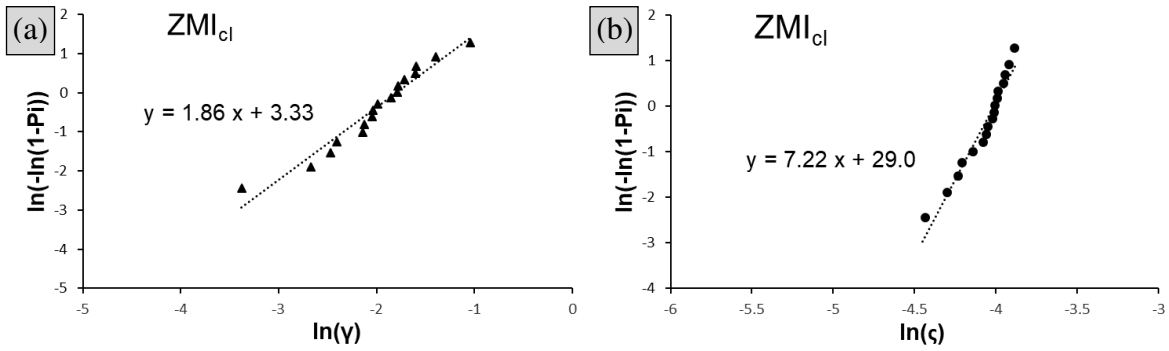

Fig. 14: Weibull representation of structural parameters (a). γ (effective section fraction with a -12% offset) and (b). ς (standard deviation of fiber load distribution) on Tyranno ZMI fiber tows that underwent a chlorination treatment.

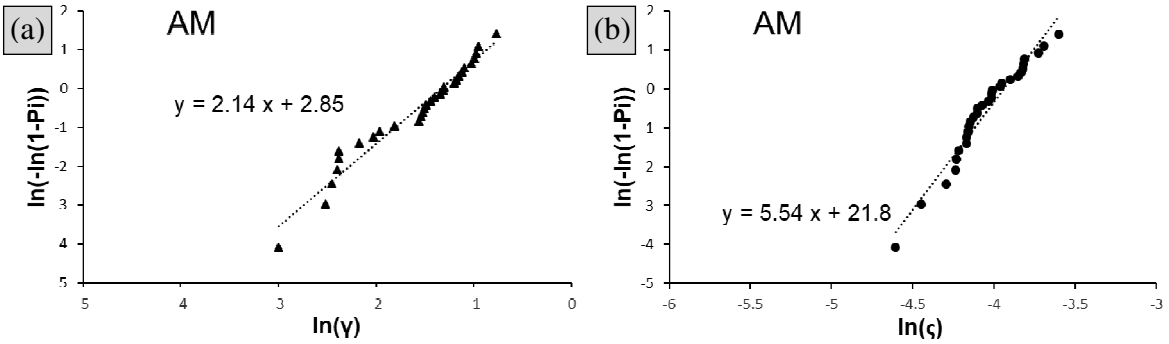

Fig. 15: Weibull representation of structural parameters (a). γ (effective section fraction with a 10% offset) and (b). ς (standard deviation of fiber load distribution) on unsized Tyranno AM fiber tows.

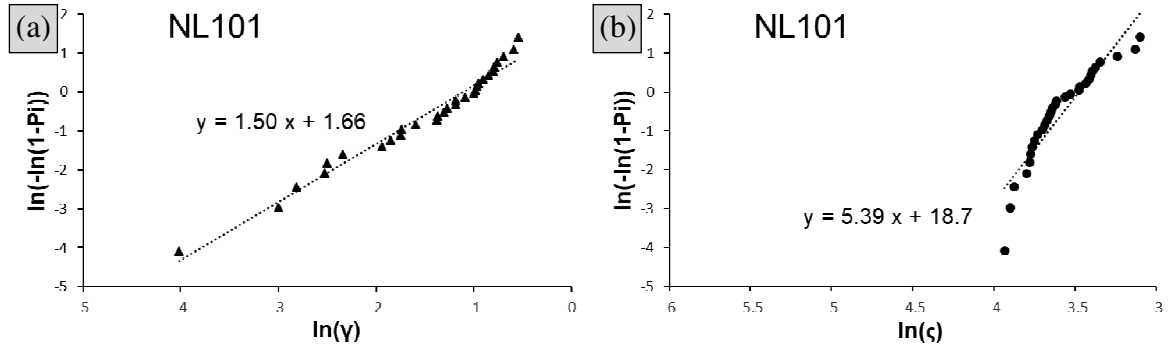

Fig. 16: Weibull representation of structural parameters (a). γ (effective section fraction with a 15% offset) and (b). ς (standard deviation of fiber load distribution) on Nicalon NL101 fiber tows.

	$\bar{\gamma}$ (%)	Me(γ) (%)	γ_{min} / γ_{max} (%)	m_γ	γ_0 (%)	$\bar{\varsigma}$ (N)	Me(ς) (N)	m_ς	ς_0 (N)
NL101	15 ± 13	14.3	-13 / 58	1.50	32.9*	0.0285	0.0262	5.39	0.0311
NL207	10 ± 10	11.1	-11 / 29	2.44	28.9*	0.0268	0.0259	6.86	0.0273
NL207*	20 ± 6.0	18.7	8.0 / 35	1.84	14.3*	0.0249	0.0250	8.70	0.0261
Hi-Ni	14 ± 12	14.3	-6.0 / 40	2.00	27.3*	0.0259	0.0260	6.93	0.0274
Hi-Ni-S	25 ± 16	21.2	1.3 / 53	1.36	29.0	0.0406	0.0399	3.53	0.0443
TS	16 ± 11.2	14.3	1.0 / 44	1.48	22.8	0.0099	0.0089	4.29	0.0097
TS11	10 ± 8.5	10.7	1.2 / 33	1.33	11.8	0.0179	0.0175	5.96	0.0186
Lox-M	25 ± 8.1	22.1	12.5 / 39	1.38	15.6*	0.0240	0.0228	5.84	0.0243
ZMI	14 ± 8.5	14.1	-3.5 / 28	2.29	23.6*	0.0211	0.0202	5.29	0.0216
ZMI‡	26 ± 6.5	26.9	14.8 / 39	1.49	13.6*	0.0198	0.0195	5.72	0.0208
ZMI_{Cl}	27 ± 8.0	25.7	15.4 / 47	1.86	16.6*	0.0169	0.0177	7.22	0.0163
AM	13 ± 11	13.1	-5.0 / 46	2.14	26.3*	0.0180	0.0171	5.54	0.0195

Table 6: Structural parameters of multifilament tows assessed by tensile testing. * indicates offsetted sets.

NL207	TS	TS	TS11	Lox-M	Hi Ni	Hi Ni
700 MPa	700 MPa	500 MPa	700 MPa	700 MPa	1000 MPa	1500 MPa
650 °C	550 °C	650 °C	650 °C	650 °C	500 °C	500 °C
1198	46500	6783	4941	1985	2612	56
1336	57861	24263	8453	2441	13438	60
2377	92667	25281	10639	2673	14052	86
3491	189835	26858	13712	3261	16195	86
3654	229358	32539	15140	8362	16386	1148
5318	232633	35879	15878	9709	29241	1300
7546	240524	53981	17196	9955	31008	2081
9975	246014	60038	17303	10775	33905	3146
13980	265345	64396	17381	16168	33957	3453
25155	272211	69012	18772	17066	34137	3866
28068	306542	73977	19621	17324	39518	4261
31732	356840	77876	20862	18649	50205	5369
42121	377509	82018	23250	18763	52700	6803
57095	386300	85795	24726	19447	56072	7240
76123	414748	87669	25074	19773	71298	11420
80393	486407	90388	25194	20339	74099	23900
91866	435313	94951	26380	21326	94451	25041
102445	509817	105047	26685	22750	100728	29709
104586	543303	111772	30591	22817	114539	31223
113737	556292	114190	32430	28079	144820	34023
124731	583611	127467	35027	28897	153422	34148
133002	648384	137948	35537	28910	182008	40071
146905	708140	140008	37545	29599	196280	40728
168832	794509	158797	40446	36163	202380	44588
176073	820232	160676	41575	36565	225628	48126
268278	864154	169464	43143	37741	278471	52695
338775	877336	196330	49534	41079	288711	89101
348401	1070683	267717	56644	41216	448951	95798
678431	1165121	501459	60575	64163	536286	109083
809030	2456843		158326	104561	647954	
					1345475	

Table 7: Lifetime (s) data under static fatigue condition for different SiC tow types. Applied stresses are given for γ = 0%.

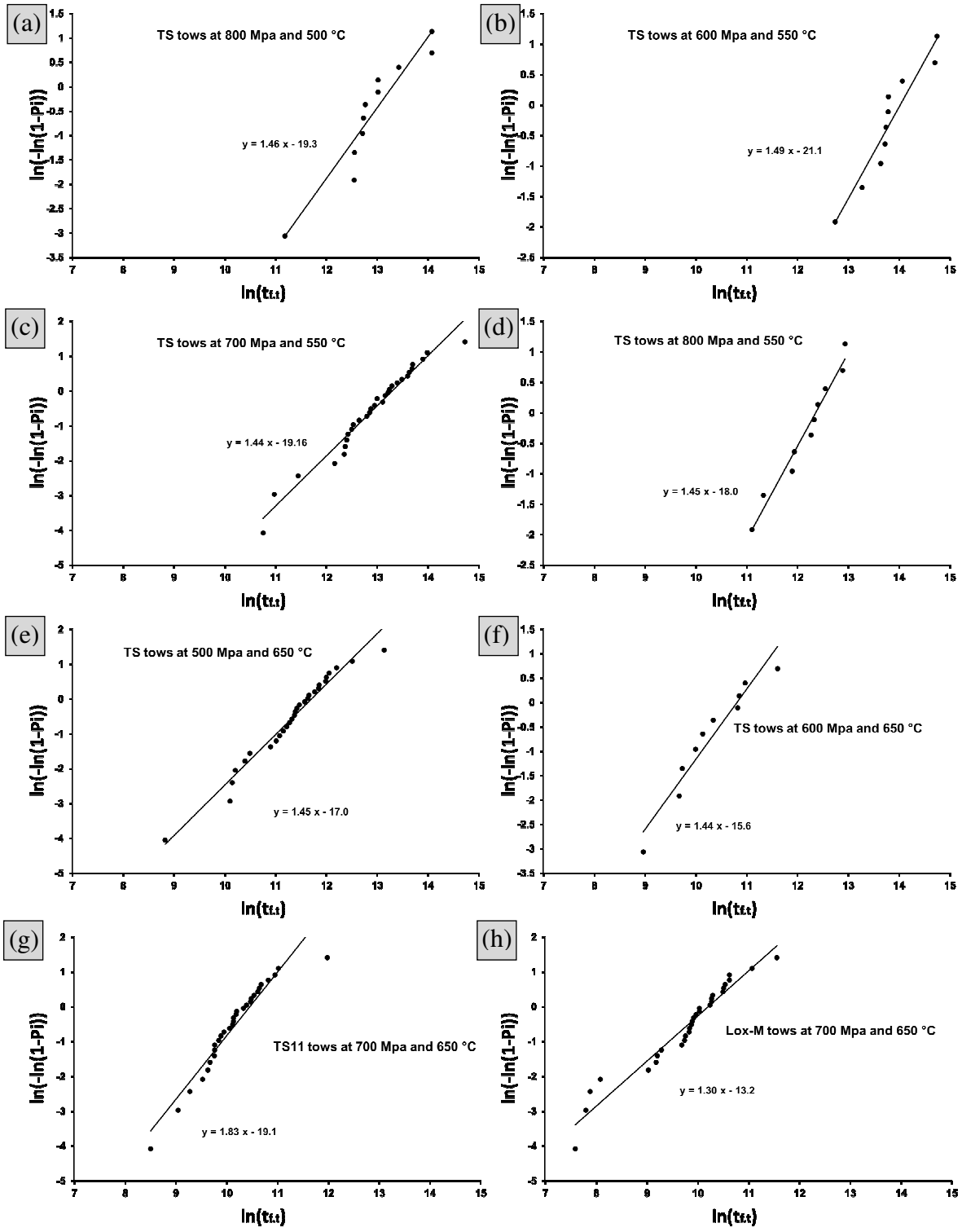
(a)
TS tows at 800 Mpa and 500 °C
y = 1.46 x - 19.3
(b)
TS tows at 600 Mpa and 550 °C
y = 1.49 x - 21.1
(c)
TS tows at 700 Mpa and 550 °C
y = 1.44 x - 19.16
(d)
TS tows at 800 Mpa and 550 °C
y = 1.45 x - 18.0
(e)
TS tows at 500 Mpa and 650 °C
y = 1.45 x - 17.0
(f)
TS tows at 600 Mpa and 650 °C
y = 1.44 x - 15.6
(g)
TS11 tows at 700 Mpa and 650 °C
y = 1.83 x - 19.1
(h)
Lox-M tows at 700 Mpa and 650 °C
y = 1.30 x - 13.2
ln(-ln(1-Pi))
ln(tf)

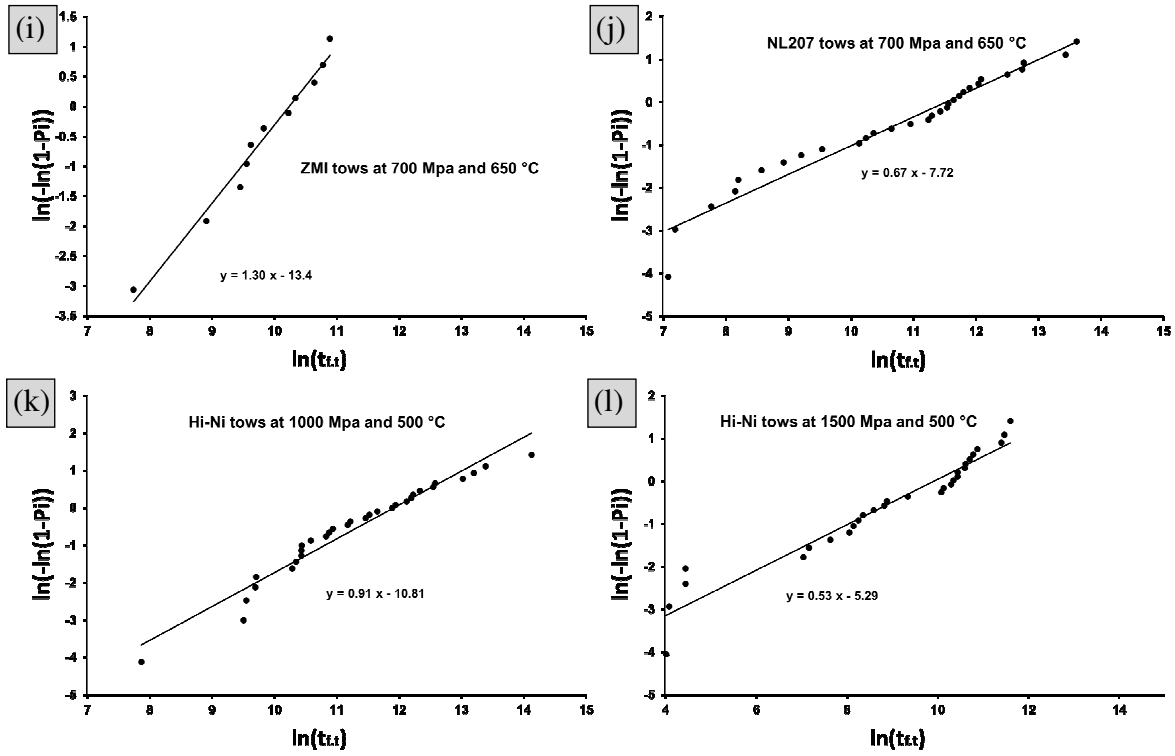

Fig. 17: Weibull distribution (Eq. (10)) of time to failure for various fiber tow types and static fatigue conditions: (a). TS 500 °C and 800 MPa (b). TS 550 °C and 600 MPa (c). TS 550 °C and 700 MPa (d). TS 550 °C and 800 MPa (e). TS 650 °C and 500 MPa (f). TS 650 °C and 600 MPa (g). TS11 650 °C and 700 MPa (h). Lox-M 650 °C and 700 MPa (i). ZMI 650 °C and 700 MPa (j). NL207 650 °C and 700 MPa (k). Hi-Ni 500 °C and 1000 MPa (l). Hi-Ni 500 °C and 1500 MPa. Stresses are given for null γ (engineering stress).

Fiber	Condition	$m_{df.t}$	t_0 (s)	Reference
NL207	700 MPa 650 °C	0.67	1.02×10^5	
Hi-Ni	1000 MPa 500 °C	0.91	1.50×10^5	[4]
Hi-Ni	1500 MPa 500°C	0.53	2.04×10^4	[4]
Hi-Ni	300MPa 900°C	0.45	2.66×10^5	[4]
Hi-Ni-S	1000 MPa 600 °C	0.78	2.06×10^5	[5]
TS	800 MPa 500 °C	1.46	5.88×10^5	
TS	600 MPa 550 °C	1.49	1.23×10^6	
TS	700 MPa 550 °C	1.44	6.05×10^5	
TS	800 MPa 550 °C	1.45	2.40×10^5	
TS	300 MPa 650 °C	1.44	1.32×10^6	
TS	500 MPa 650 °C	1.45	1.20×10^5	
TS	600 MPa 650 °C	1.44	4.93×10^4	
TS	700 MPa 650 °C	1.44	4.67×10^4	[6]
TS11	700 MPa 650 °C	1.83	3.50×10^4	
Lox-M	700 MPa 650 °C	1.30	2.66×10^4	
ZMI	700 MPa 650 °C	1.30	5.45×10^5	
ZMI‡	910 MPa 650°C	0.78	2.76×10^4	
ZMI‡	910 MPa 550°C	0.84	2.54×10^5	

Table 8: Distribution of SiC-based tows static fatigue experimental data at various conditions, temperature or applied stress, interpreted by Weibull statistic (Eq. (10)).

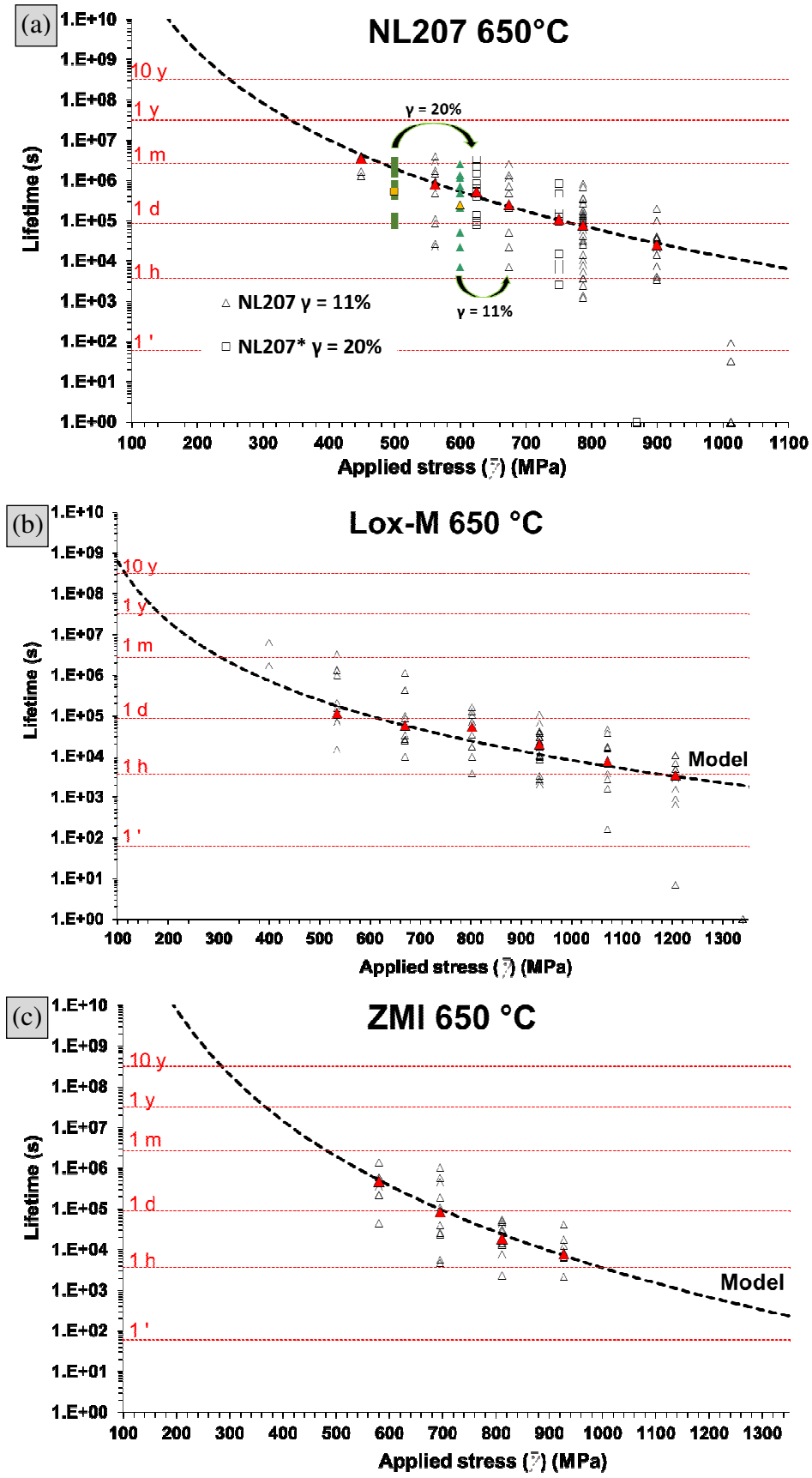

Fig. 18: Endurance diagrams for (a). NL207, (b). Lox-M and (c). ZMI tows at 650 °C. The correction of the applied stress using γ is highlighted on NL207.

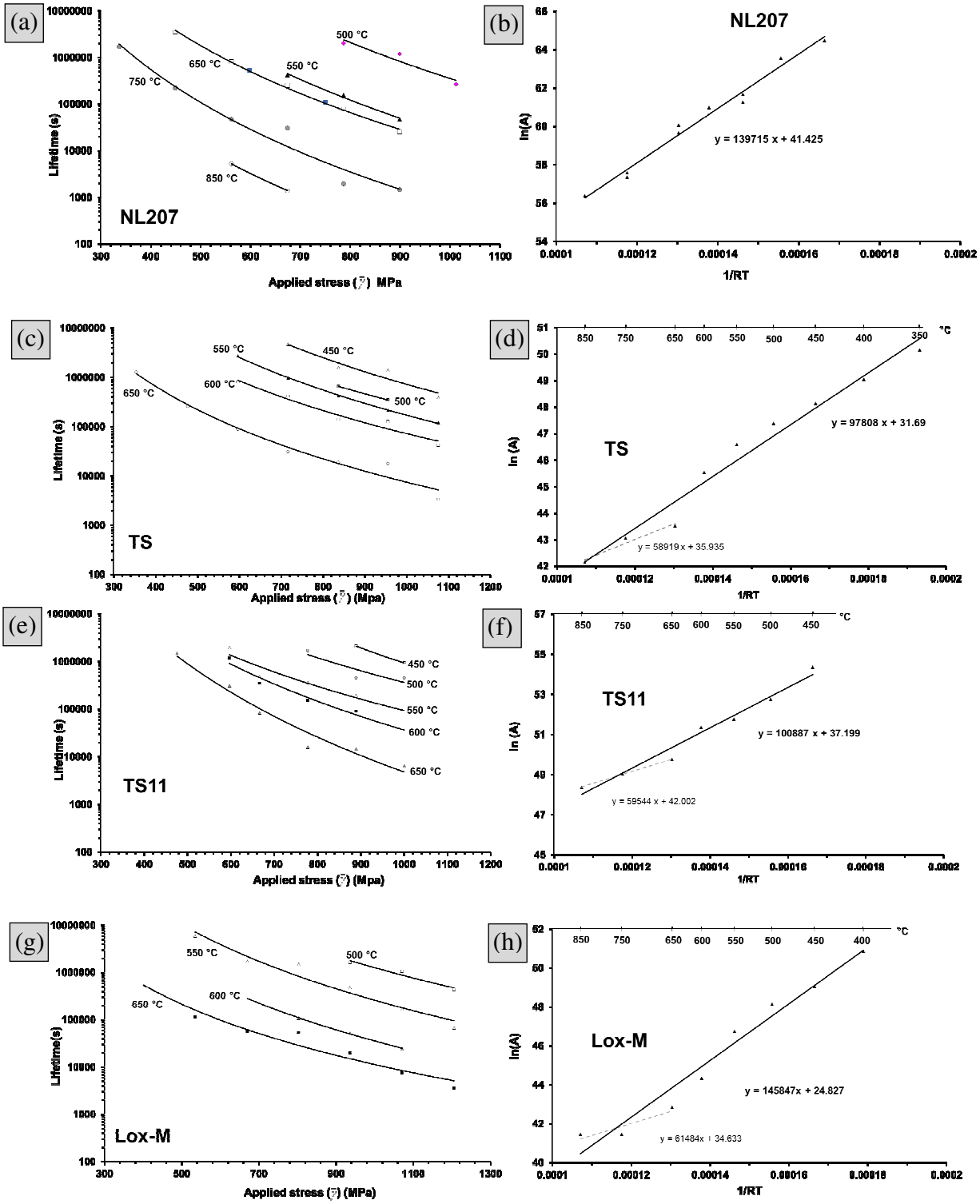
(a)
NL207
500 °C
650 °C
550 °C
750 °C
850 °C
Lifetime (s)
Applied stress (σ) MPa
(b)
NL207
y = 139715 x + 41.425
ln(A)
1/RT
(c)
TS
550 °C
450 °C
600 °C
650 °C
500 °C
Lifetime (s)
Applied stress (σ) (Mpa)
(d)
TS
y = 97808 x + 31.69
y = 58919 x + 35.935
ln (A)
1/RT
°C
(e)
TS11
450 °C
500 °C
550 °C
600 °C
650 °C
Lifetime (s)
Applied stress (σ) (Mpa)
(f)
TS11
y = 100887 x + 37.199
y = 59544 x + 42.002
ln (A)
1/RT
°C
(g)
Lox-M
550 °C
500 °C
650 °C
600 °C
Lifetime(s)
Applied stress (σ) (MPa)
(h)
Lox-M
y = 145847x + 24.827
y = 61484x + 34.633
ln(A)
1/RT
°C

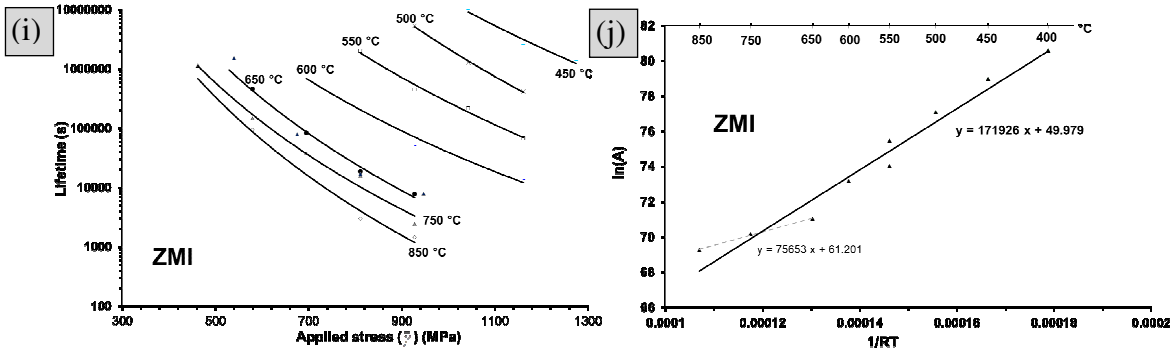

Fig. 19: Endurance diagrams (median lifetimes) and Arrhenius plots for (a,b). NL207 (c,d). TS (e,f). TS11 (g,h). Lox-M and (i,j). ZMI tows under static fatigue conditions.

T (°C)	NL207		Hi-Ni		Hi-Ni-S		TS		TS11		Lox-M		ZMI	
	n	A x 10^{25} (s $MPa^{7.3}$)	*n*	A x 10^{26} (s $MPa^{8.4}$)	*n*	A x 10^{25} (s $MPa^{7.2}$)	*n*	A x 10^{19} (s $MPa^{5.0}$)	n	A x 10^{21} (s $MPa^{5.8}$)	*n*	A x 10^{19} (s $MPa^{4.9}$)	*n*	A x 10^{31} (s $MPa^{9.1}$)
350	-	-	-	-	-	-	-	600	-	-	-	-	-	-
400	-	-	-	-	-	-	-	200	-	-	-	1200	9.99	10000
450	-	1000	-	-	-	-	5.59	80	6.87	400	-	20	9.99	2000
500	6.92	400	8.45	10000	-	5700	4.81	38	5.34	80	4.67	80	11.35	300
550	7.66	40			-	-	5.26	17	4.68	30	5.49	20	9.24	60
600	-	30	-	400	7.25	250	4.84	6.0	5.48	20	5.17	1.8	8.37	6.0
650	7.05	15	-	-	-	-	4.34	0.80	6.81	4.0	4.25	0.40	8.71	0.70
700		-	-	32	-	20	-	-	-	-	-	-	-	-
750	7.63	1.0	-	-	-	-	5.29	0.50	-	2.0	-	0.10	8.39	0.30
800	-	-	8.34	4.0	7.24	2.7	-	-	-	-	-	-	-	-
850	7.25	0.30	-	-	-	-	-	0.20	-	1.0	-	0.10	9.16	0.12
900	-	-	-	0.70	-	-	-	-	-	-	-	-	-	-
550 (2)	-	60	-	-	-	-	-	-	-	-	-	-	-	14
650 (2)	7.23	8.0	-	-	-	-	-	-	-	-	-	-	7.28	0.70
750 (2)	-	0.80	-	-	-	-	-	-	-	-	-	-	-	-
$\overline{n}$	**7.3**		**8.4**		**7.2**		**5.0**		**5.8**		**4.9**		**9.1**	

Table 9: Lifetime prediction parameters, empirical power law (Eq. (8)), describing the median lifetime of SiC-based tows under static fatigue conditions at constant force and various temperatures: (i). assessment of n_t coefficients at temperatures with sufficient data, (ii). extraction of its mean value and (iii). estimation of A parameters considering the latter. NL207* and ZMI‡ noted (2).

2. Experimental Design, Materials and Methods

2.1 Material

Three generations of SiC-based fibers are commercially available, synthesized by the conversion of polycarbosilane and commercialized by Nippon carbon Co. Ltd. or UBE Industries Ltd. In this dataset, 6 first-generation fibers are reported: Nicalon® NL101, Nicalon® NL207, Tyranno® Grade S, referred as TS, Tyranno® Lox-M, Tyranno® ZMI and Tyranno® AM. Hi-Nicalon (named Hi-Ni) belongs to the second-generation whereas Hi-Nicalon Type S (named Hi-Ni-S) is a third generation SiC-based fiber completing the work. Two different batches of NL207 (NL207 and NL207*) and TS (TS and TS11, with 8.5 and 11 µm respective diameters) tows were characterized. Unsized and chlorinated ZMI tows were also examined, originating from the same batch. The formers were heat treated at 650 °C for 10 min in air. The latter were unsized, followed by thin silica film removal in 10 vol.% hydrofluoric acid bath for 4 minutes, dried and then treated under pure chlorine at 650 °C for 40 min, method described elsewhere [1-3].

2.1 Method

Tensile tests on bundles were conducted on hot grips probes also used for static fatigue testing [6]. Sized bundles of 300 mm length were weighted for average cross sectional area determination (Eq. (2)), and positioned in alumina tube grips. To ensure probe alignment, a pre-load was applied and maintained by fugitive Loctite® glue. A solution of dissolved PMMA was applied on the 25 mm gauge length separating grips, to avoid capillarity cement transportation during curing. Tubes were finally filled with alumina based thermostructural cement (Ceramabond 503, Polytec PI) and cured at 370 °C for 2 hours. Tensile tests were carried out on non-lubricated yarns at a constant displacement rate of 50 µm min^{-1} (strain rate of 0.2 % min^{-1}). Prior to ruin behavior assessment, the early loading stage was cycled (0-30 N, in the elastic domain) in order to align the fibers. It is worth noting further cycling did not improved fiber parallelism (Fig. 1b). Elongations were measured by two LVDT extensometers mounted on the grips. For system compliance assessment, three (3) more tests at 60 mm and 100 mm gauge lengths were carried out. The engineering stress applied to the bundle was corrected taking the fraction of unloaded fibers (γ Eq. (3)) into account (Eq. (1)). 30 tests were conducted to assess the distribution parameters, excepting for Hi-Ni-

S (Table 2) and ZMI_{Cl} (Table 4) with 26 and 18 tests respectively. A total of 100 tests were however conducted on TS tows [6] for a more extensive dispersion assessment.

$$\sigma_\gamma = \frac{w_t}{S_t(1-\gamma)} \quad (1)$$

with $$S_t = \frac{m_0}{L_0 \rho} \quad (2)$$

and $$\gamma = 1 - \frac{N_0}{N_t} = 1 - \frac{E_t}{E_f} \quad (3)$$

Where m_0 is the tow mass and ρ the fibers density (Table 1). w_t is the applied force (N, mass x 9.81 m s^{-2}), N_0 the initial number of intact filaments and N_t its total manufactured number (500, 800 or 1600). Finally, E_t and E_f are respectively monofilament (Table 1) and tow Young's moduli.

Models to describe the failure of bundles were originally proposed by H.E. Daniels [7] and B.D. Coleman [8] on following hypotheses: a bundle is composed of N_0 fibers (supposed equal to N_t), identical, continuous, parallel and equally loaded. If the damage tolerant failure behavior of multifilament tows has overwhelmingly been exploited to extract strength distribution of filaments [9-11], such load displacement curves comprise another helpful information although seldomly reported: the initial shape of the curve (upward curvature Fig. 1) revealing the fiber slack [12,13]. This latter induce a filament load distribution (Fig. 4): $w_{fj} = \overline{w}_f + \delta_{Fj}$, where w_{fj} is the load applied to the j^{th} filament, $\overline{w}_f$ its mean value corresponding to the tow one ($\overline{w}_f = w_t / N_0$) and δ_{Fj} the load distribution (over or underload on j^{th} filament). The section fraction carrying the force ($\psi_{(t)}$), inferred from Eq. (4) assuming homogeneous elastic modulus and fiber diameter, progressively increases until 100% when the N_0 fibers are loaded (linear evolution of force-strain). This was experimentally evidenced below 30 N.

$$\psi_{(t)} = 1 - \frac{\Delta F_{(t)}}{F_{(t)} + \Delta F_{(t)}} \quad (4)$$

Where $\Delta F_{(t)}$ the difference between the applied force and its theoretical value considering the linearity reached at 30 N (Fig. 3a).

Each force increment, applied to the full sample, is carried by N_t x (1 - γ) x $\psi_{(t)}$ fibers. Cumulative incremental force was used to define the distribution of filament load (δ_F, in N). The latter is considered independent to the global load, which means a fiber overloaded by δ_F = 50 mN during the initial stage will always be until its failure. This is obviously independent to reloading phenomenon when filaments fail. A normal distribution (Eq. (5)), with $\overline{w}_f$ as mean value and standard deviation referred as ς, was selected to describe δ_F sliding distribution (Fig. 3b). To facilitate the understanding and interpretation, this load distribution can then implicitly be converted in stress (Fig. 4), assuming the N_0 fibers have a constant cross section ($\overline{S}_f$). From this point of view, the average stress applied to fibers corresponds to the stress on tow ($\sigma_{app.t(\overline{\gamma})}$) with ς / $\overline{S}_f$ as standard deviation.

$$f(\delta_F) = \frac{1}{\varsigma\sqrt{2\pi}} \exp\left[-\frac{\left(\delta_F - \frac{w_t}{N_t(1-\gamma)} \right)^2}{2\varsigma^2} \right] \quad (5)$$

Where ς is the standard deviation of load applied to filaments and w_t the load applied to the tow.

In this data article, Weibull statistical distributions were ascribed to above described structural parameters (γ and ς), implicitly revoking their discrete nature (Eqs. (6),(7)). Linear least squares method was used to assess the modulus and characteristic value. The relevancy of this statistical law was evaluated with the Kolmogorov–Smirnov test [14].

$$\varsigma = \varsigma_0 \ln\left(\frac{1}{1-P_\varsigma} \right)^{\frac{1}{m_\varsigma}} \quad (6)$$

Where P_ς is the probability of ς for a given tow, m_ς and ς_0 Weibull distribution parameters.

$$\gamma = \gamma_0 \ln\left(\frac{1}{1-P_\gamma} \right)^{\frac{1}{m_\gamma}} \quad (7)$$

Where P_γ is the probability of γ for a given tow, m_γ and γ_0 the Weibull statistical parameters.

As shown in tables 2-4,6, negative γ values could in some cases be extracted from bundle tensile test, meaning a Young modulus on tow exceeding the fiber one (Eq. (3)). Two (2) approximations can here be pointed to explain such non-intuitive behavior: (i). over-

estimation of filament Young modulus which shows some variability or (ii). under-estimation of bundle section (Eq. (2)), averaged (based on weight and density) on a 300 mm long sample among which only 25 mm were effectively tested. This latter explanation is more likely to explain these negative γ values, thus not aberrant but method related. Consequently, and to take such values into account in distributions, some data set were offsetted for statistical parameters assessment (Figs. 5-7,11-16).

Static fatigue testing used the hot grip technique to ensure a uniform temperature along the entire specimen gauge length. The applied dead weight (w_t) was adjusted with respect to the desired engineering tow test stress (Eq. (1)). The dead weight was suspended to inferior grip turning a timer on. Heating-up (20 °C min^{-1}) was then initiated and its duration subtracted from lifetime when relevant. The automatic stop of timer when specimen failed gave the tow lifetime. Were deemed as valid only those tests that run without breakage during the initial step of load application. Because force and strain could not be recorded, the actual γ value of the tested tow could not be estimated for the evaluation of applied stress. Its average value (Table 6) was hence used. Prediction parameters assessment was based on endurance diagrams, constructed plotting median lifetime versus applied stress. Therefore, a discrete stress scanning approach with 11 tests conducted at each condition was applied. Distribution of lifetime were estimated on larger set sizes (30 or more tests) in one single condition.

Time to failure ($t_{f.t}$) of bundles was demonstrated to follow a Paris type law, simplified by a power relationship relating $t_{f.t}$ to the applied stress (σ) (Eq. (8)) [15]. A and *n* are respectively the environment constant, related to the environment temperature by an Arrhenius law (Eq. (9) with Ea_{SCG} the SCG apparent activation energy, A_0 the pre exponential constant, R = 8.314 J K^{-1} mol^{-1}) and *n* the stress corrosion susceptibility factor.

$$t_{f.t} = A\,\sigma^{-n} \quad (8)$$

$$A = A_0 e^{\frac{Ea_{SCG}}{RT}} \quad (9)$$

Lifetime variability can nicely be described using the Weibull statistic (Eq. (10)) [1,4,6,16], where $t_{f.t0}$ is the characteristic time to failure and $m_{df.t}$ the static fatigue Weibull modulus. These parameters were also assessed by linear least square method applied to Weibull plots.

$$P_i = 1 - e^{-\left(\frac{t_{f.t}}{t_{f.t0}}\right)^{m_{df.t}}} \quad (10)$$

Declaration of Competing Interest

The authors declare that they have no known competing financial interests or personal relationships which have, or could be perceived to have, influenced the work reported in this article.

References

[1] S. Mazerat, A. Delcamp, R. Pailler, J. Lamon, H. Plaisantin, Improvement of silicon carbide fibers mechanical properties by Cl2 etching, J. Eur. Ceram. Soc. 38(16) (2018) 5301−5310.
doi: 10.1016/j.jeurceramsoc.2018.06.026

[2] S. Mazerat, J. Lacroix, B. Rufino R. Pailler, Carbon derived from silicon carbide fibers, a comparative study, Mater. Today Com. 19 (2019) 177–185.
doi: 10.1016/j.mtcomm.2019.01.013

[3] S. Mazerat, G. Puyoo, G. Chollon, F. Teyssandier, R. Pailler, S. Loison, E. Philippe, Composition and reactivity of various silicon carbide fibers, HTCMC8 Ceram. Trans. 248 (2014) 113–123.
doi: 10.1002/9781118932995.ch13

[4] A. Laforet, Rupture différée en fatigue statique aux très hautes températures (800°C-1300°C) des fils Hi-Nicalon, des composites Hi-Nicalon/type PyC/SiC et des composites Hi-Nicalon/type PyC/B4C, PhD Thesis, University of Bordeaux, France (2009).

[5] W. Gauthier, Rupture différée en fatigue statique aux températures intermédiaires (<800°C) de fils et de fibres à base de carbure de silicium, PhD Thesis, University of Bordeaux, France (2006).

[6] S. Mazerat, A. Delehouze, R. Pailler, Delayed failure prediction of SiC-based bundles: the impact of sampling size, Int. J. Fatigue 138 (2020) 105694.
doi: 10.1016/j.ijfatigue.2020.105694

[7] H.E. Daniels, The statistical theory of the strength of bundles of threads. I, Proc. Royal Soc. 138 (1945) 405−435.
doi: 10.1098/rspa.1945.0011

[8] B.D. Coleman, On the strength of classical fibers bundle, J. Mech. Phys. Solids 7 (1958) 60−70.
doi: 10.1016/0022-5096(58)90039-5

[9] M. R'Mili, T. Bouchaour, P. Merele, Estimation of Weibull parameters from loose-bundle tests, Comp. Sci. Technol. 56 (1996) 831−834.
doi: 10.1016/0266-3538(96)00028-0

[10] Z. Chi, T.W. Chou, G. Shen, Determination of single fibre strength distribution from fibre bundle testings, J. Mater. Sci. 19 (1984) 3319−3324.
doi: 10.1007/BF00549820

[11] M. R'Mili, M. Moevus, N. Godin, Statistical fracture of E-glass fibres using a bundle tensile test and acoustic emission monitoring, Comp. Sci. Technol. 68(7−8) (2008) 1800−1808.
doi: 10.1016/j.compscitech.2008.01.018

[12] S.L. Phoenix, Probabilistic strength analysis of fibre bundle structures, Fibre Sci. Technol. 7 (1974) 15−31.
doi: 10.1016/0015-0568(74)90003-7

[13] V. Calard, J. Lamon, Failure of fiber bundles, Comp. Sci. Tech. 64 (2004) 701−710.
doi: 10.1016/j.compscitech.2003.07.003

[14] K.C. Datsiou, M. Overend, Weibull parameter estimation and goodness-of-fit for glass strength data, Struct. Safety, 73 (2018), 29−41.
doi: 10.1016/j.strusafe.2018.02.002

[15] W. Gauthier, J. Lamon, Delayed Failure of Hi-Nicalon and Hi-Nicalon S multifilament tows and single filaments at intermediate temperatures (500°-800°C), J. Am. Ceram. Soc. 92(3) (2009) 702−709.
doi: 10.1111/j.1551-2916.2009.02924.x

[16] R. Danzer, T. Lube, P. Supancic, R. Damani, Fracture of ceramics, Adv. Eng. Mater. 10(4) (2008) 275−298.
doi: 10.1002/adem.200700347

Figure captions

Fig. 1: Load displacement curve for (a). TS bundle tensile test highlighting the damage tolerant failure mode and (b). cycling in 0-30 N range on a ZMI tow.

Fig. 2: Weibull plots for bundle tensile strength of (a). Nicalon NL101 (b). Nicalon NL207 (c). Nicalon NL207* (second batch) (d). Hi-Nicalon (e). Hi-Nicalon type S (f). Tyranno Grade S 8.5 µm mean diameter (g). Tyranno Grade S 11 µm mean diameter (h). Tyranno Lox-M (i). Tyranno ZMI (j). Tyranno ZMI‡ (desized) (k). Tyranno ZMI_{Cl} (chlorinated) (l). Tyranno AM.

Fig. 3: (a). Initial loading of a Hi-Ni tow (0-30 N range), used to estimate the load distribution (b). derived from deviation to linearity. On this example, ς = 0.026 N, $\overline{w}_f$ = 0.075 N and γ = 22%.

Fig. 4: Distribution of stress applied to Hi-Ni fibers considering the structural aspects: effective section ($\bar{\gamma}$) and fiber slacking with 3 different standard deviations (ς) corresponding to a probability of 0.01, 0.5 and 0.99 on the Weibull distribution (Eq. (6)).

Fig. 5: Weibull representation of structural parameters (a). γ (effective section fraction with a 15% offset) and (b). ς (standard deviation of fiber load distribution) on Nicalon NL207 fiber tow.

Fig. 6: Weibull representation of structural parameters (a). γ (effective section fraction with a -7% offset) and (b). ς (standard deviation of fiber load distribution) on Nicalon NL207 fiber tow.

Fig. 7: Weibull representation of structural parameters (a). γ (effective section fraction with a 10% offset) and (b). ς (standard deviation of fiber load distribution) on Hi-Nicalon fiber tow.

Fig. 8: Weibull representation of structural parameters (a). γ (effective section fraction) and (b). ς (standard deviation of fiber load distribution) on Hi-Nicalon-S fiber tow.

Fig. 9: Weibull representation of structural parameters (a). γ (effective section fraction) and (b). ς (standard deviation of fiber load distribution) on Tyranno Grade S (8.5 µm diameter, TS) fiber tow.

Fig. 10: Weibull representation of structural parameters (a). γ (effective section fraction) and (b). ς (standard deviation of fiber load distribution) on Tyranno Grade S (11 µm diameter, TS11) fiber tow.

Fig. 11: Weibull representation of structural parameters (a). γ (effective section fraction with a -12% offset) and (b). ς (standard deviation of fiber load distribution) on Tyranno Lox-M fiber tow.

Fig. 12: Weibull representation of structural parameters (a). γ (effective section fraction with a 7% offset) and (b). ς (standard deviation of fiber load distribution) on Tyranno ZMI fiber tow.

Fig. 13: Weibull representation of structural parameters (a). γ (effective section fraction with a -14% offset) and (b). ς (standard deviation of fiber load distribution) on unsized Tyranno ZMI fiber tow.

Fig. 14: Weibull representation of structural parameters (a). γ (effective section fraction with a -12% offset) and (b). ς (standard deviation of fiber load distribution) on Tyranno ZMI fiber tow that underwent a chlorination treatment.

Fig. 15: Weibull representation of structural parameters (a). γ (effective section fraction with a 10% offset) and (b). ς (standard deviation of fiber load distribution) on unsized Tyranno AM fiber tow.

Fig. 16: Weibull representation of structural parameters (a). γ (effective section fraction with a 15% offset) and (b). ς (standard deviation of fiber load distribution) on Nicalon NL101 fiber tow.

Fig. 17: Weibull distribution (Eq. (10))of time to failure for various fiber tow types and static fatigue conditions: (a). TS 500 °C and 800 MPa (b). TS 550 °C and 600 MPa (c). TS 550 °C and 700 MPa (d). TS 550 °C and 800 MPa (e). TS 650 °C and 500 MPa (f). TS 650 °C and 600 MPa (g). TS11 650 °C and 700 MPa (h). Lox-M 650 °C and 700 MPa (i). ZMI 650 °C and 700 MPa (j). NL207 650 °C and 700 MPa (k). Hi-Ni 500 °C and 1000 MPa and (l). Hi-Ni 500 °C and 1500 MPa. Stresses are given for null γ (engineering stress).

Fig. 18: Endurance diagrams for (a). NL207, (b). Lox-M and (c). ZMI tows at 650 °C. The correction of the applied stress using γ is highlighted on NL207.

Fig. 19: Endurance diagrams (median lifetimes) and Arrhenius plots for (a,b). NL207 (c,d). TS (e,f). TS11 (g,h). Lox-M and (I,j). ZMI tows under static fatigue conditions at various temperatures under ambient air.

Figures

Fig.1

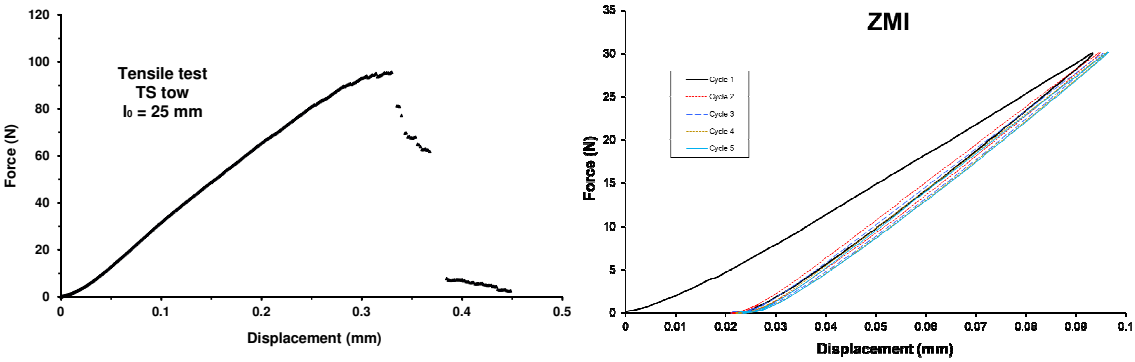

Fig.2

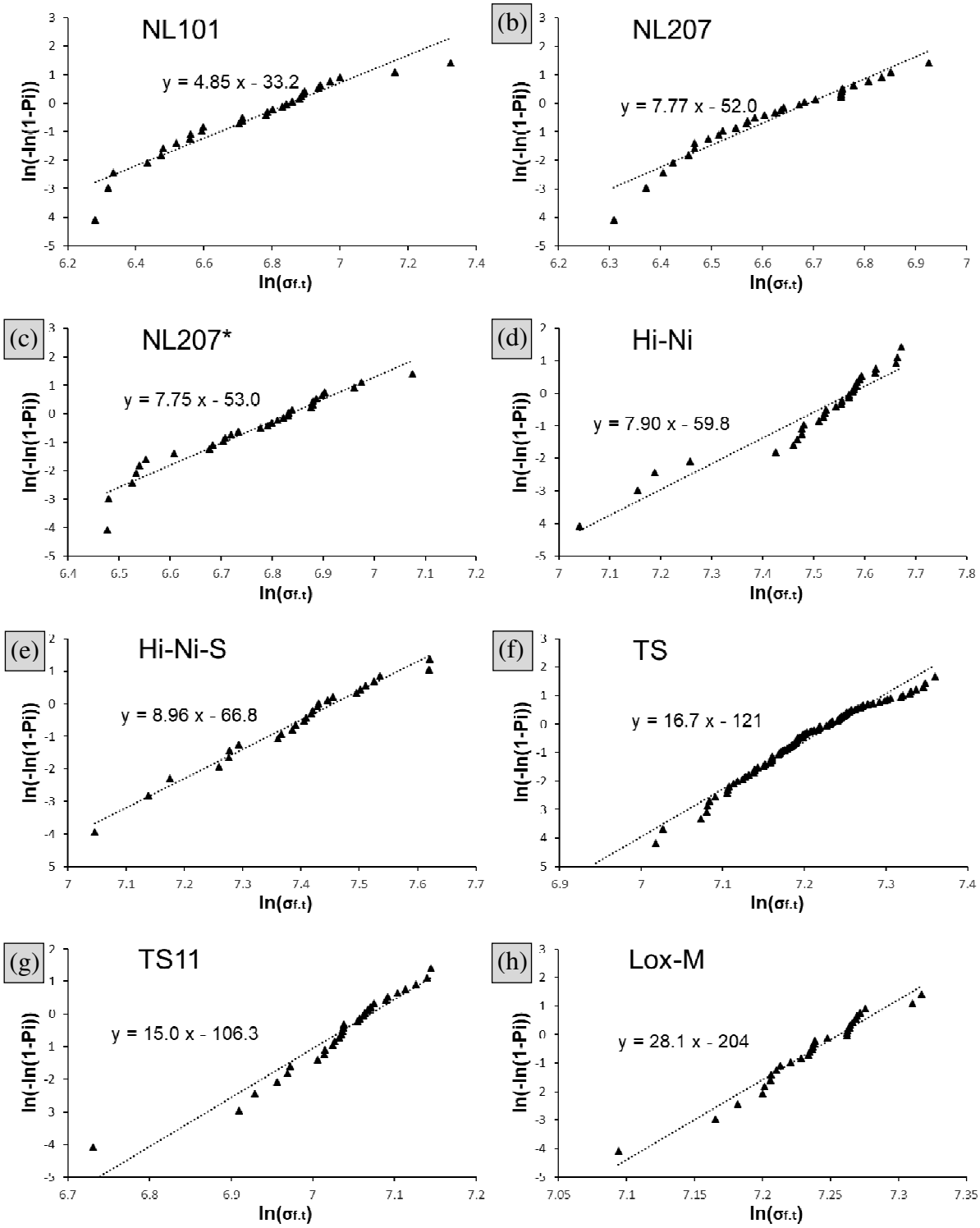
NL101
y = 4.85 x - 33.2
(b)
NL207
y = 7.77 x - 52.0
(c)
NL207*
y = 7.75 x - 53.0
(d)
Hi-Ni
y = 7.90 x - 59.8
(e)
Hi-Ni-S
y = 8.96 x - 66.8
(f)
TS
y = 16.7 x - 121
(g)
TS11
y = 15.0 x - 106.3
(h)
Lox-M
y = 28.1 x - 204
ln(-ln(1-Pi))
ln(σf.t)

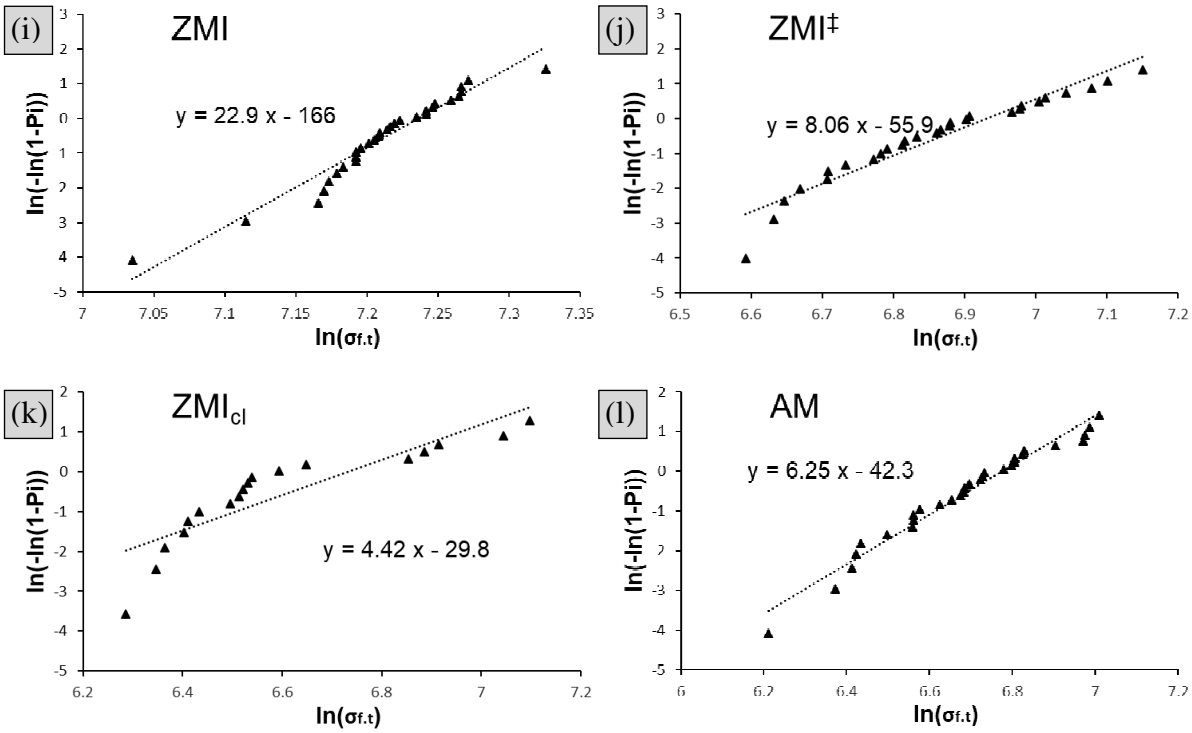
(i)
ZMI
y = 22.9 x - 166
ln(-ln(1-Pi))
ln(σf.t)
(j)
ZMI‡
y = 8.06 x - 55.9
ln(-ln(1-Pi))
ln(σf.t)
(k)
ZMIcl
y = 4.42 x - 29.8
ln(-ln(1-Pi))
ln(σf.t)
(l)
AM
y = 6.25 x - 42.3
ln(-ln(1-Pi))
ln(σf.t)

Fig.3

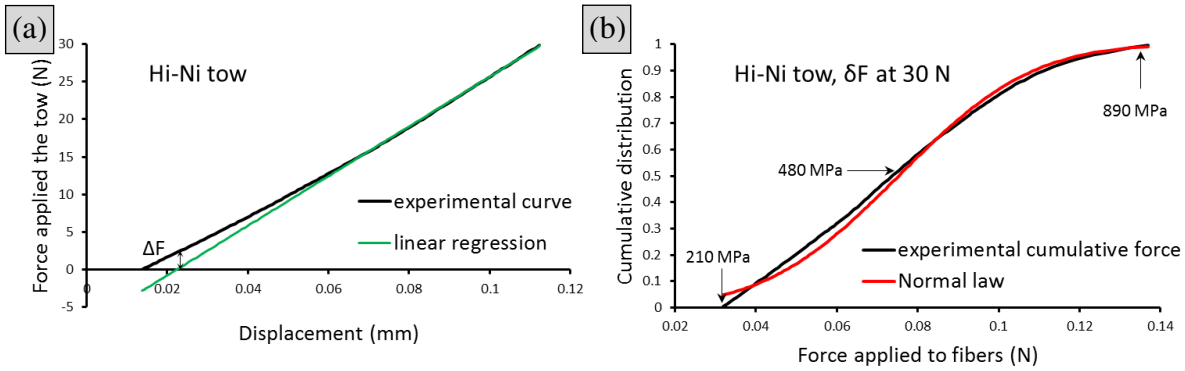
(a)
Hi-Ni tow
Force applied the tow (N)
Displacement (mm)
ΔF
experimental curve
linear regression
(b)
Hi-Ni tow, δF at 30 N
Cumulative distribution
Force applied to fibers (N)
210 MPa
480 MPa
890 MPa
experimental cumulative force
Normal law

Fig.4

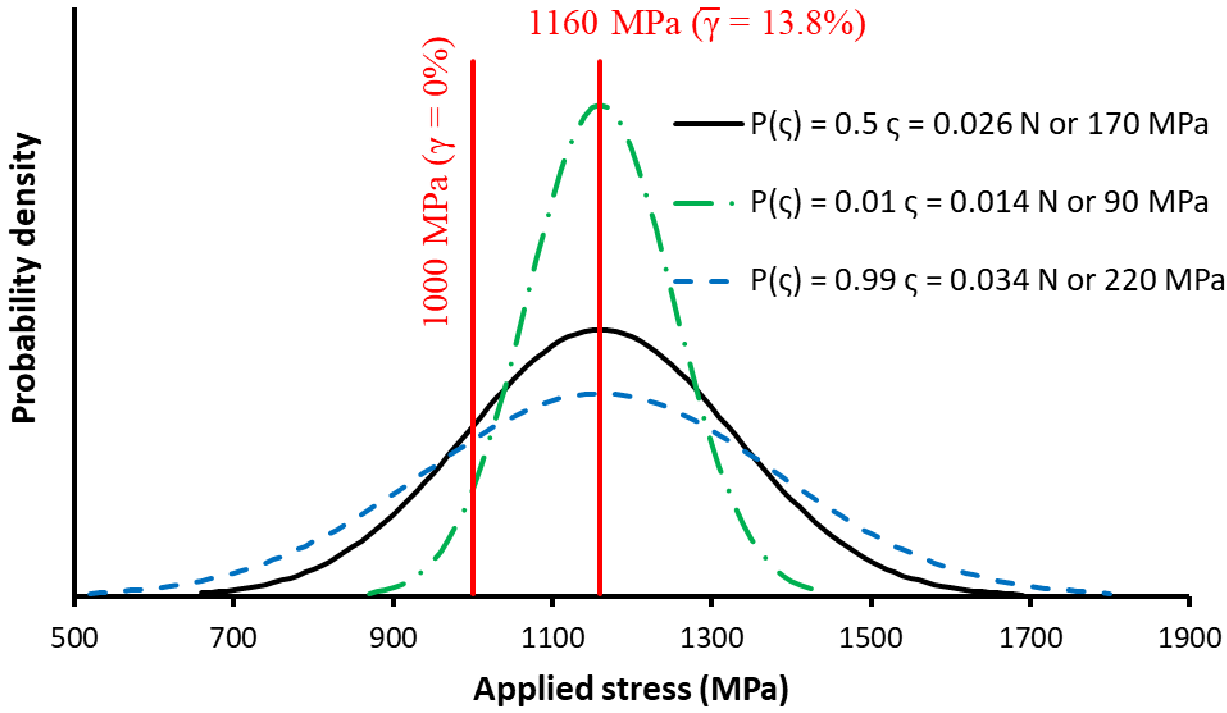
1160 MPa ($\bar{\gamma}$ = 13.8%)
1000 MPa (γ = 0%)
P(ς) = 0.5 ς = 0.026 N or 170 MPa
P(ς) = 0.01 ς = 0.014 N or 90 MPa
P(ς) = 0.99 ς = 0.034 N or 220 MPa
Probability density
500
700
900
1100
1300
1500
1700
1900
Applied stress (MPa)

Fig. 5

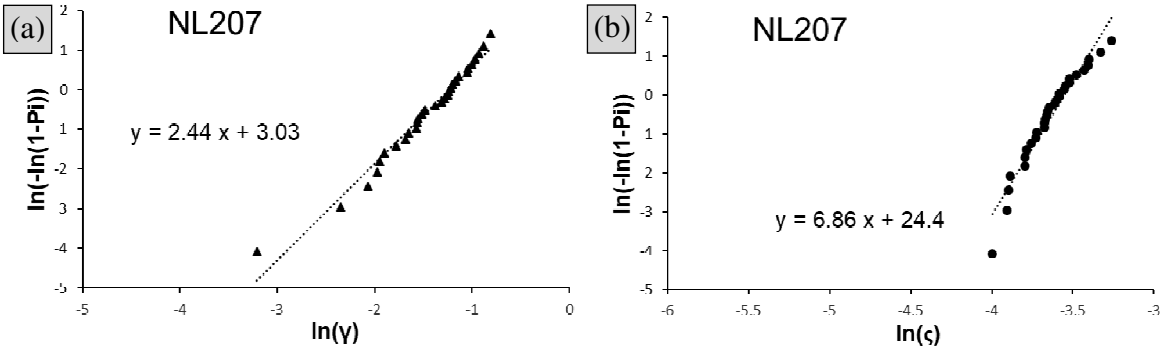

Fig. 6

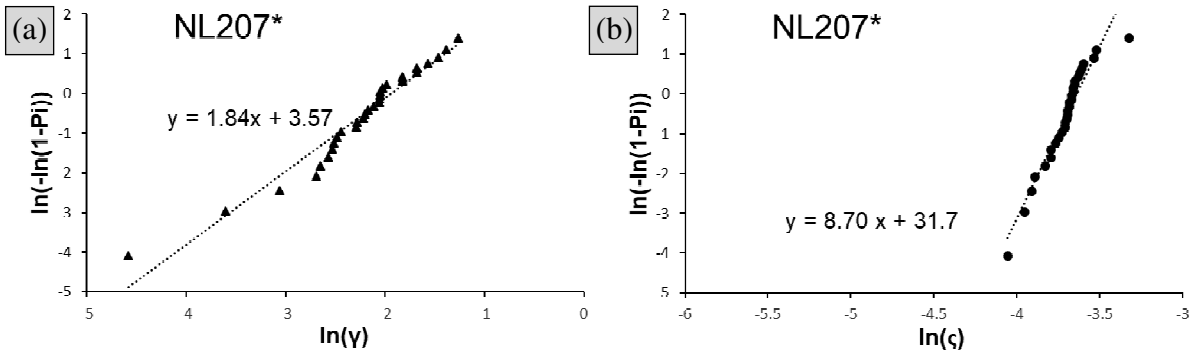

Fig. 7

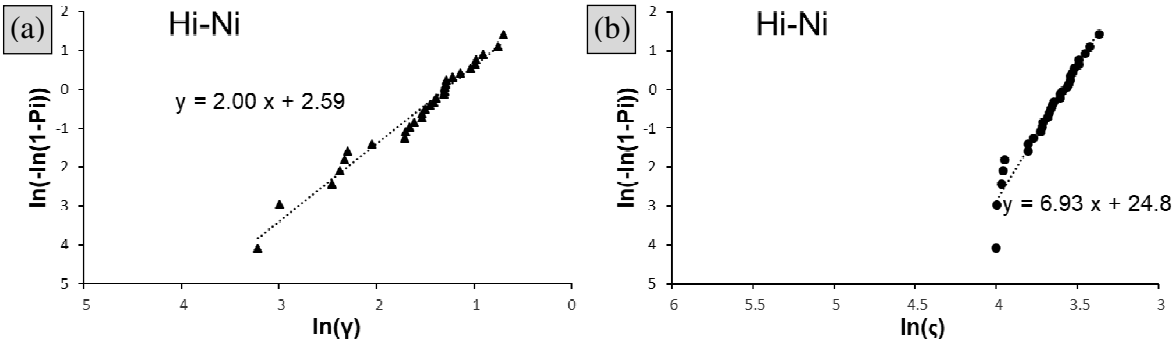

Fig. 8

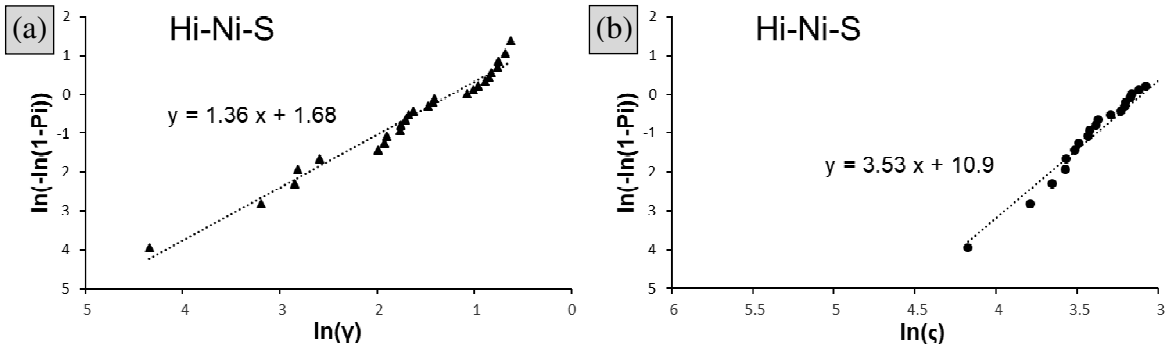

Fig. 9

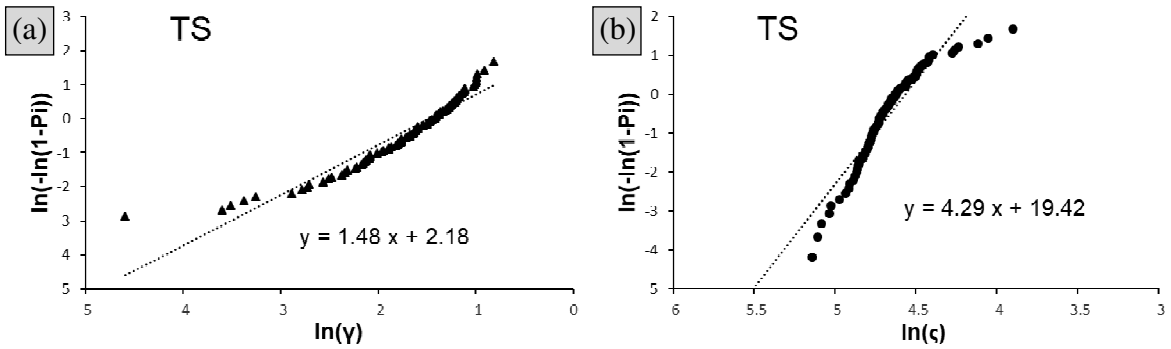

Fig. 10

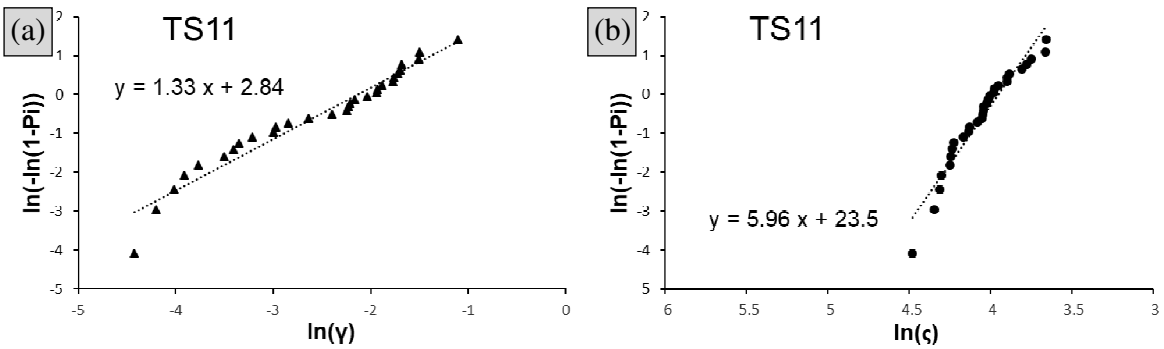

Fig. 11

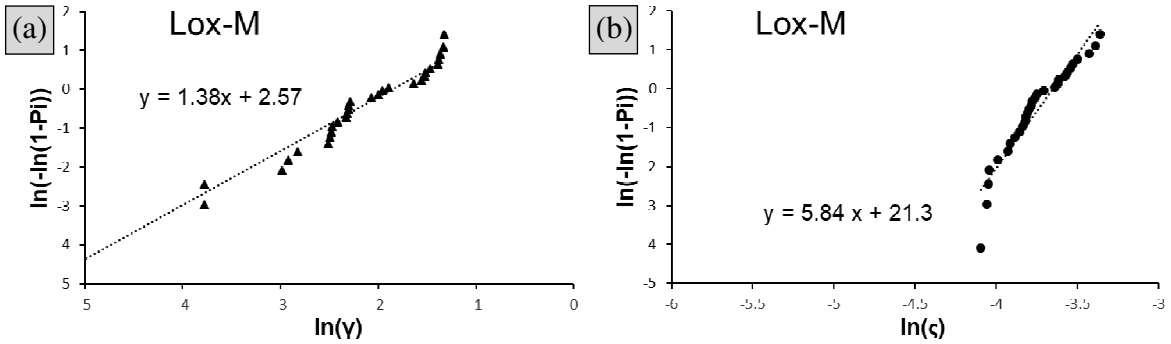

Fig. 12

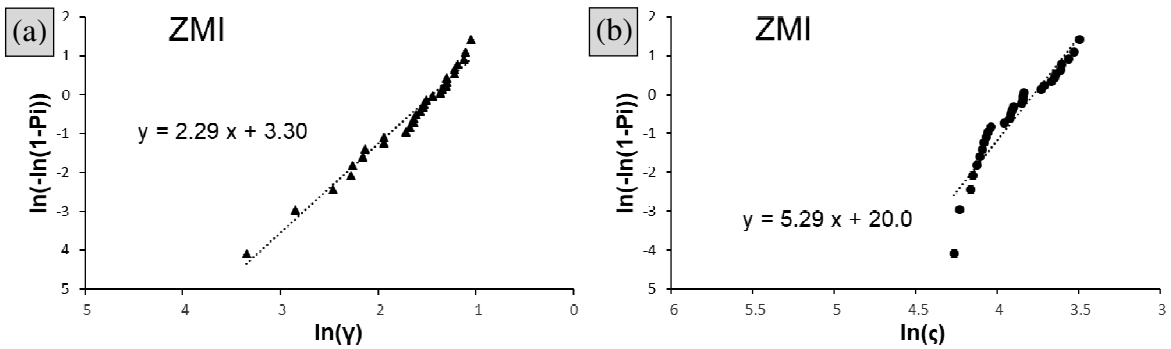

Fig. 13

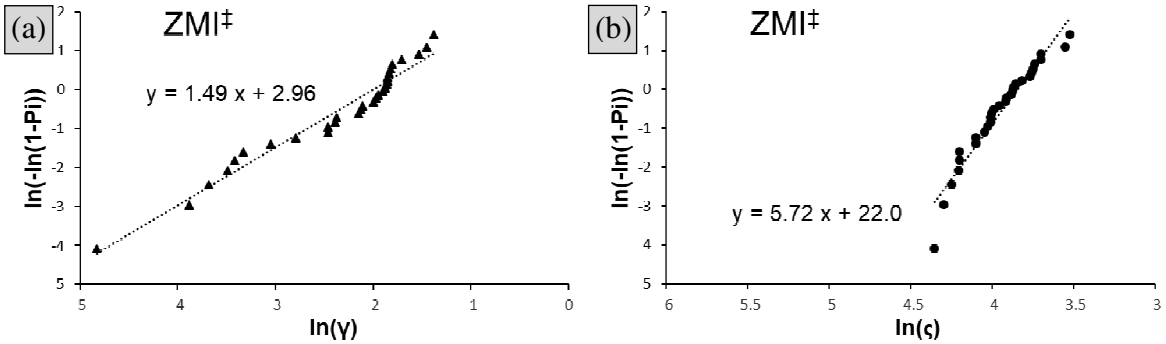

Fig. 14

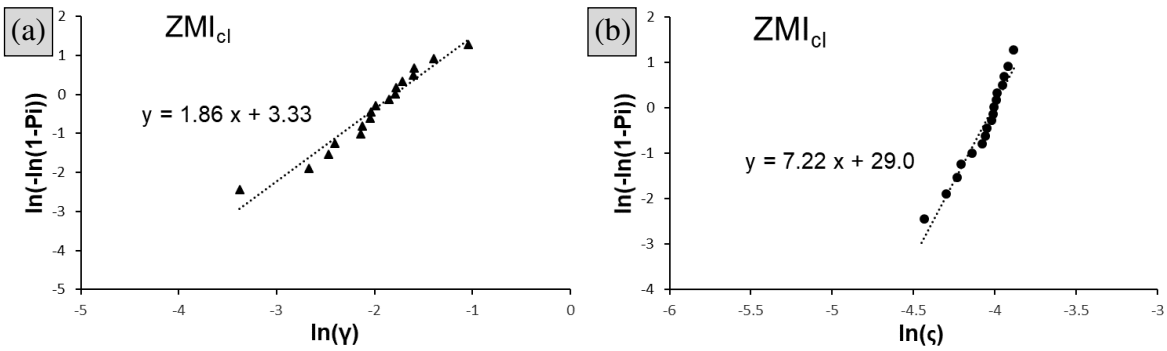

Fig. 15

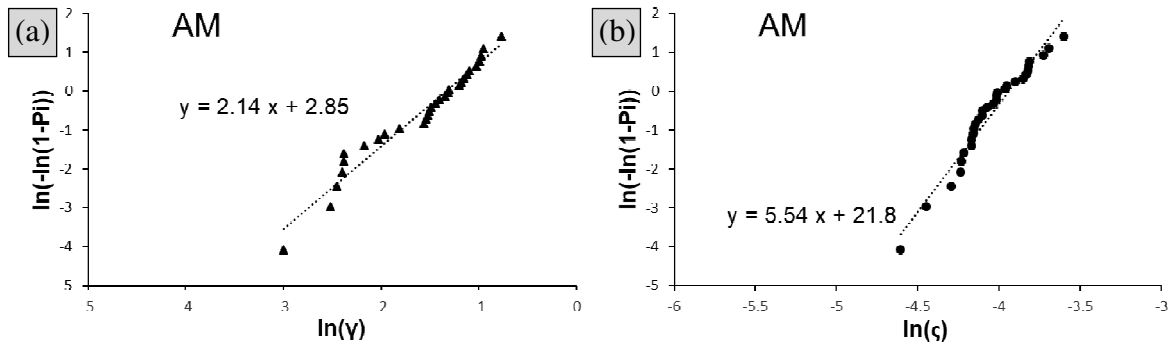

Fig. 16

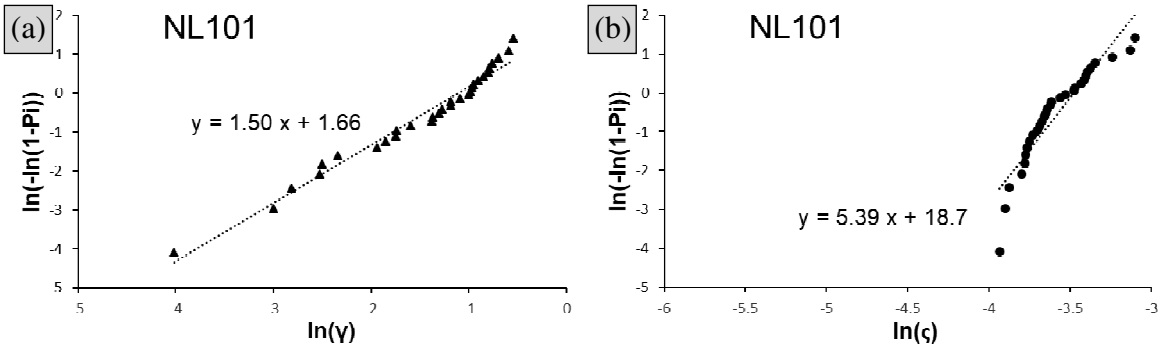

Fig. 17

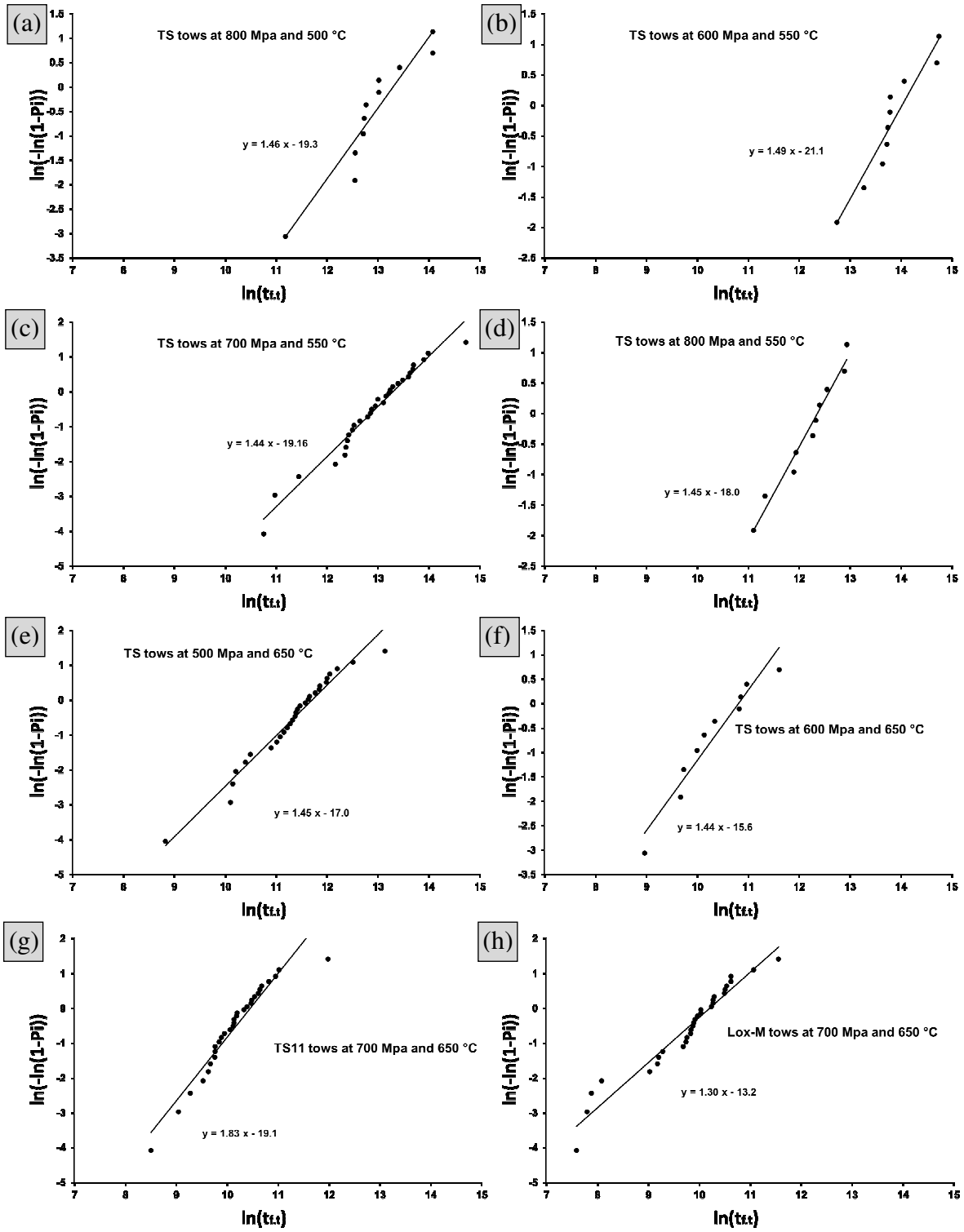
(a)
TS tows at 800 Mpa and 500 °C
y = 1.46 x - 19.3
(b)
TS tows at 600 Mpa and 550 °C
y = 1.49 x - 21.1
(c)
TS tows at 700 Mpa and 550 °C
y = 1.44 x - 19.16
(d)
TS tows at 800 Mpa and 550 °C
y = 1.45 x - 18.0
(e)
TS tows at 500 Mpa and 650 °C
y = 1.45 x - 17.0
(f)
TS tows at 600 Mpa and 650 °C
y = 1.44 x - 15.6
(g)
TS11 tows at 700 Mpa and 650 °C
y = 1.83 x - 19.1
(h)
Lox-M tows at 700 Mpa and 650 °C
y = 1.30 x - 13.2
ln(-ln(1-Pi))
ln(tf)

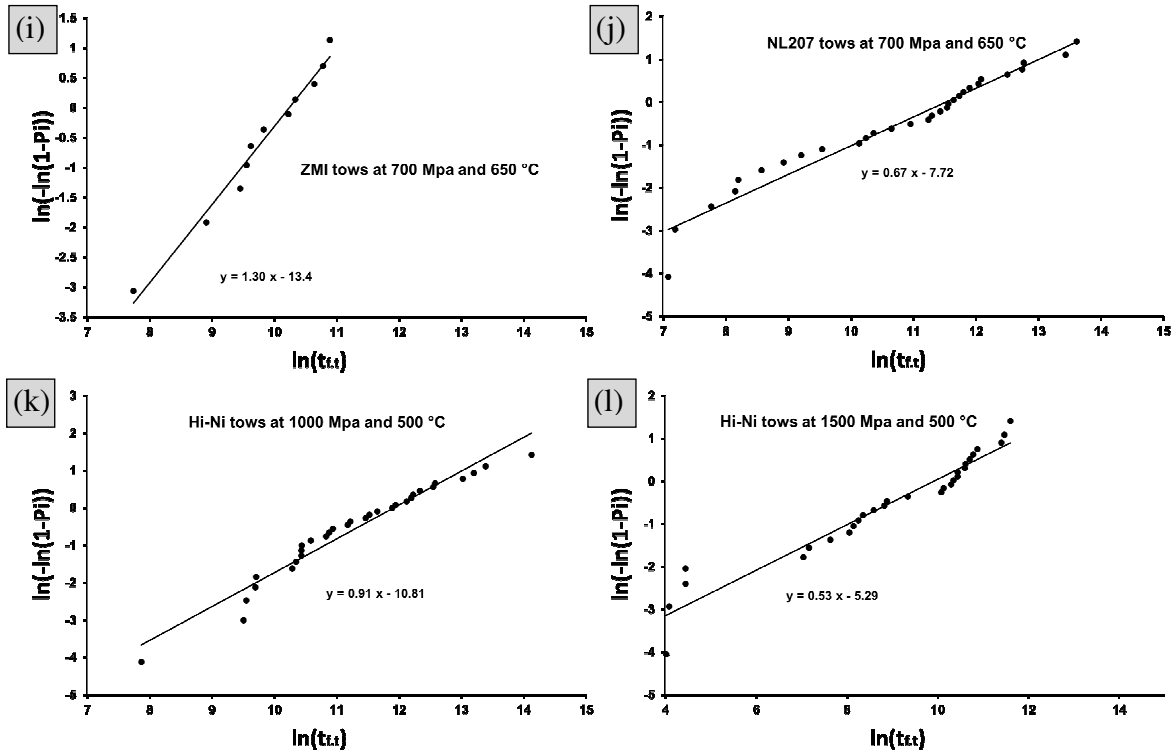
(i)
ZMI tows at 700 Mpa and 650 °C
y = 1.30 x - 13.4
ln(-ln(1-Pi))
ln(tf,i)
(j)
NL207 tows at 700 Mpa and 650 °C
y = 0.67 x - 7.72
ln(-ln(1-Pi))
ln(tf,i)
(k)
Hi-Ni tows at 1000 Mpa and 500 °C
y = 0.91 x - 10.81
ln(-ln(1-Pi))
ln(tf,i)
(l)
Hi-Ni tows at 1500 Mpa and 500 °C
y = 0.53 x - 5.29
ln(-ln(1-Pi))
ln(tf,i)

Fig. 18

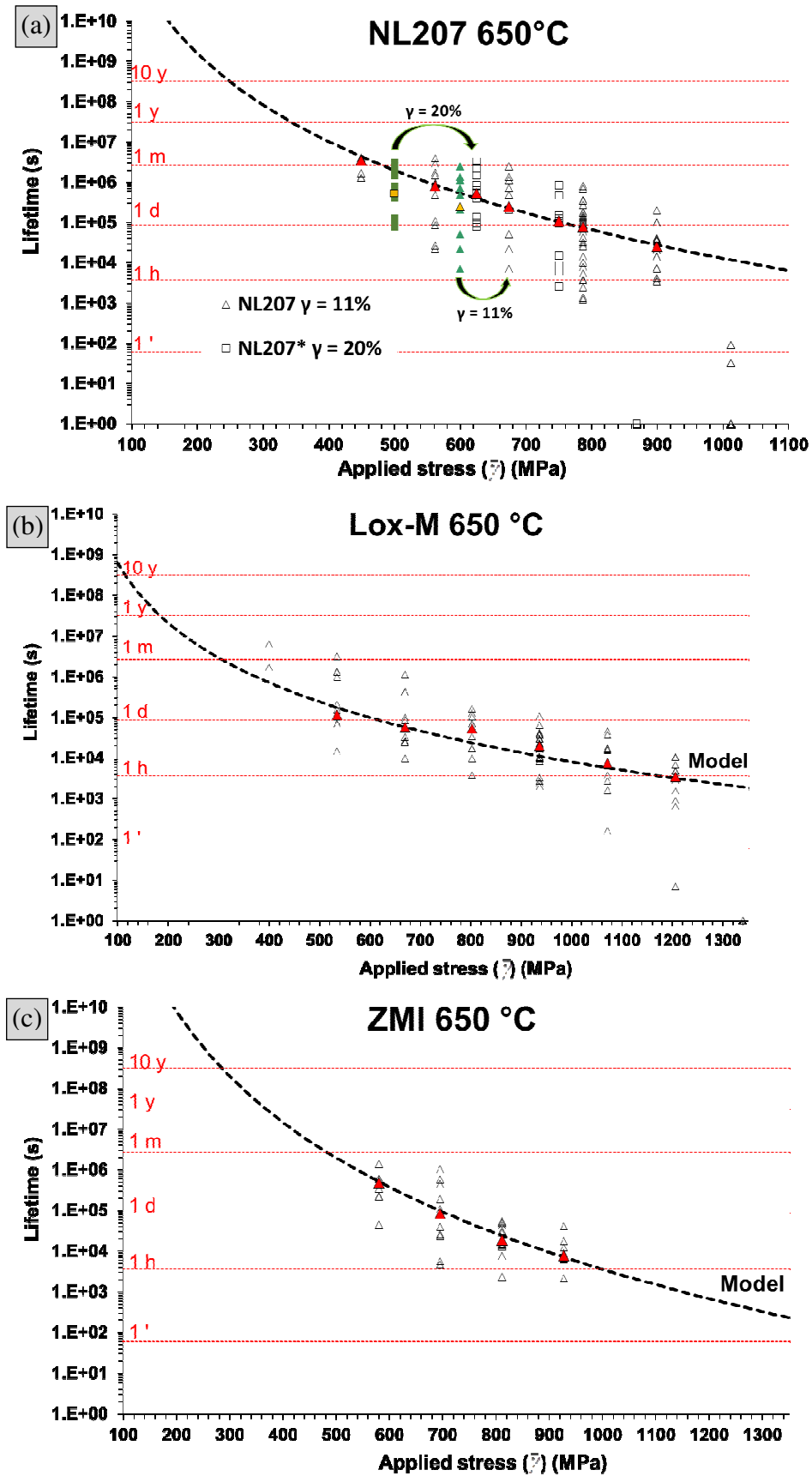
(a)
NL207 650°C
Lifetime (s)
Applied stress (σ) (MPa)
10 y
1 y
1 m
1 d
1 h
1 '
γ = 20%
γ = 11%
NL207 γ = 11%
NL207* γ = 20%
(b)
Lox-M 650 °C
Model
(c)
ZMI 650 °C
Model

Fig. 19

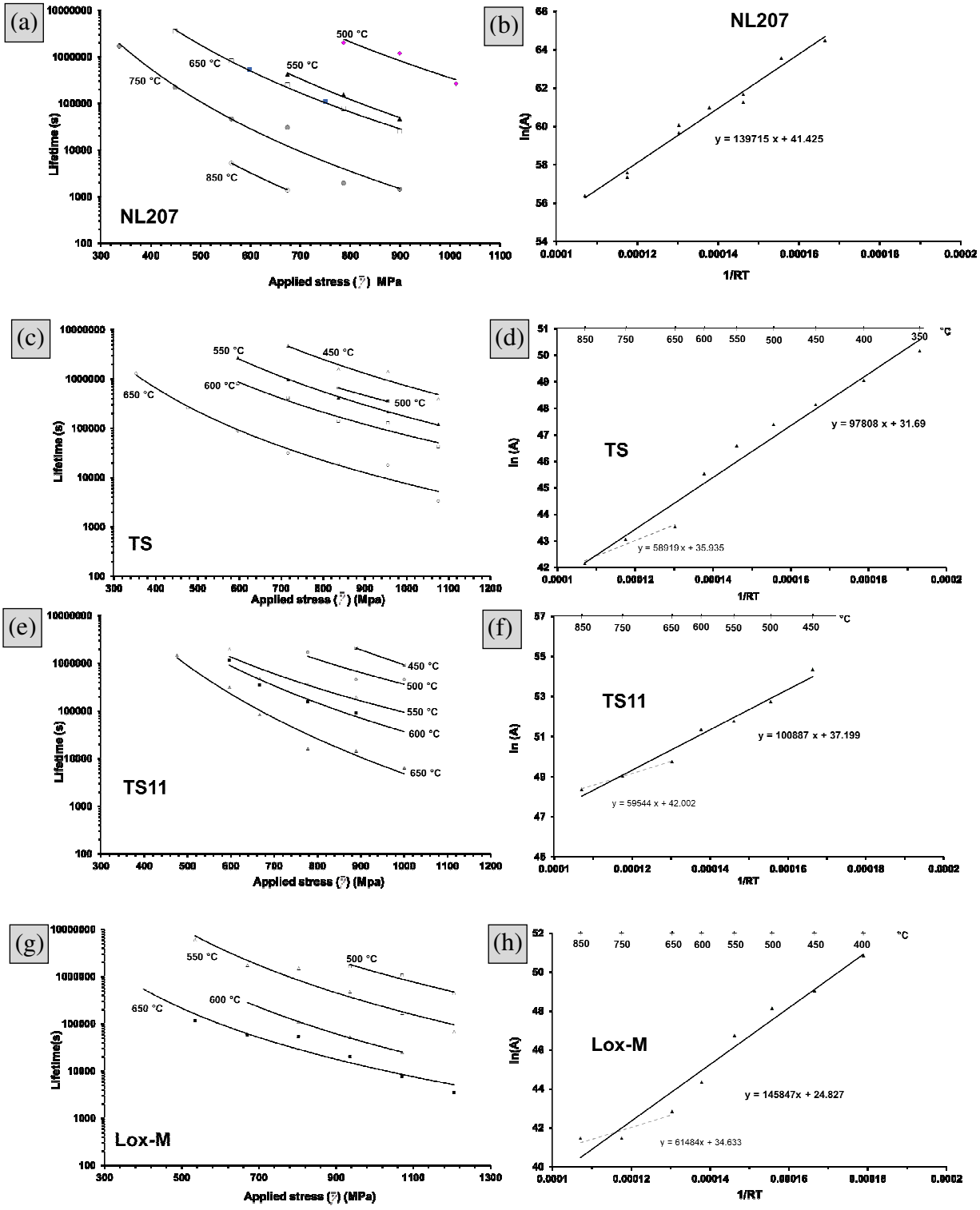
(a)
Lifetime (s)
Applied stress (σ) MPa
500 °C
550 °C
650 °C
750 °C
850 °C
NL207
(b)
NL207
ln(A)
1/RT
y = 139715 x + 41.425
(c)
Lifetime (s)
Applied stress (σ) (Mpa)
550 °C
450 °C
600 °C
650 °C
500 °C
TS
(d)
ln (A)
1/RT
°C
TS
y = 97808 x + 31.69
y = 58919 x + 35.935
(e)
Lifetime (s)
Applied stress (σ) (Mpa)
450 °C
500 °C
550 °C
600 °C
650 °C
TS11
(f)
ln (A)
1/RT
°C
TS11
y = 100887 x + 37.199
y = 59544 x + 42.002
(g)
Lifetime(s)
Applied stress (σ) (MPa)
550 °C
500 °C
650 °C
600 °C
Lox-M
(h)
ln(A)
1/RT
°C
Lox-M
y = 145847x + 24.827
y = 61484x + 34.633

(i)

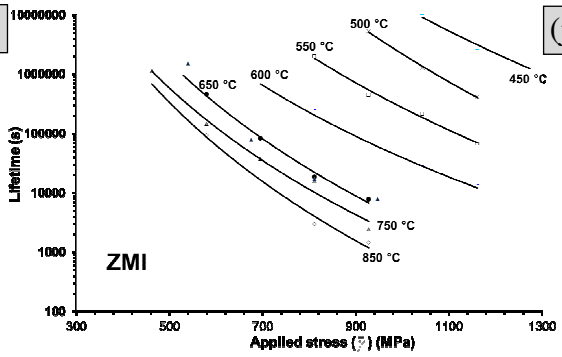
Lifetime (s)
10000000
1000000
100000
10000
1000
100
300
500
700
900
1100
1300
Applied stress (σ) (MPa)
500 °C
550 °C
600 °C
650 °C
450 °C
750 °C
850 °C
ZMI

(j)

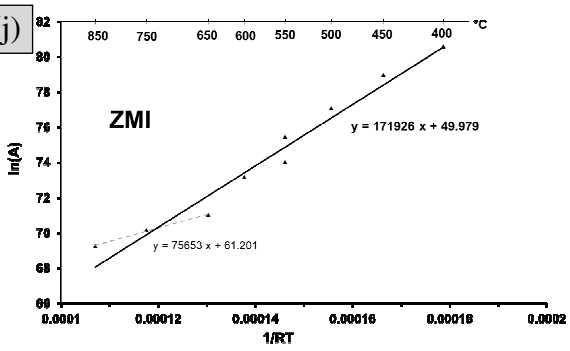
850
750
650
600
550
500
450
400
°C
ln(A)
82
80
78
76
74
72
70
68
66
ZMI
y = 171926 x + 49.979
y = 75653 x + 61.201
0.0001
0.00012
0.00014
0.00016
0.00018
0.0002
1/RT

Table captions

Table 1: Physical and mechanical properties of filaments. Sized and unsized ZMI filaments are not differentiated.

Table 2: Raw data for the tensile behavior of Hi-Ni, Hi-Ni-S and NL207 bundles.

Table 3: Raw data for the tensile behavior of TS11, Lox-M and ZMI bundles.

Table 4: Raw data for the tensile behavior of NL207*, ZMI‡ and ZMI$_{Cl}$ bundles.

Table 5: Mechanical properties of SiC-based multifilament tows.

Table 6: Structural parameters of multifilament tows assessed by tensile testing. * indicates offsetted sets.

Table 7: Lifetime (s) data under static fatigue condition for different SiC tow types. Applied stresses are given for γ = 0%.

Table 8: Distribution of SiC-based tows static fatigue experimental data at various conditions, temperature or applied stress, interpreted by Weibull statistic (Eq. (10)).

Table 9: Lifetime prediction parameters, empirical power law (Eq. (8)), describing the median lifetime of SiC-based tows under static fatigue conditions at constant force and various temperatures: (i). assessment of n_t coefficients at temperatures with sufficient data, (ii). extraction of its mean value and (iii). estimation of A parameters considering the latter. NL207* and ZMI‡ noted (2).

Table 1

Fiber	Density ($g\ cm^{-3}$)	$\sigma_{f.f}$ ± std. dev. (MPa)	E_f (GPa)	m_f	$\sigma_{1.f}$ (MPa)	K_{IC} (MPa $m^{1/2}$)	Compliance (µm N^{-1})
NL101	2.57	2166 ± 559	180	4.28	2390	1.20	48
NL207	2.58	2839 ± 667	210	5.05	3090	1.20	43
NL207*	2.58	2672 ± 710	210	4.35	2950	1.20	20
Hi-Ni	2.74	3136 ± 368	300	9.84	3295	1.66	24
Hi-Ni-S	3.05	2877 ± 414	410	8.42	3062	1.86	110
TS	2.35	3152 ± 624	180	8.17	3550	1.11	180
TS11	2.35	2776 ± 647	180	4.79	3034	1.12	170
Lox-M	2.37	2984 ± 695	200	4.63	3314	1.11	86
ZMI	2.48	3076 ± 742	200	4.81	3372	1.01	150
ZMI_{Cl}	2.48	4039 ± 479	220	9.99	4265	1.01	115
AM	2.42	2815 ± 533	180	5.74	3024	1.20	84

Table 2

Hi-Ni			Hi-Ni-S			NL207		
γ	$\sigma_{f.f(\gamma)}$	ς	γ	$\sigma_{f.f(\gamma)}$	ς	γ	$\sigma_{f.f(\gamma)}$	ς
0.029	2125	0.0183	0.534	1665	0.0740	0.076	790	0.0173
0.081	1955	0.0231	0.363	1448	0.0569	0.058	724	0.0252
0.195	1323	0.0251	0.381	1148	0.0589	0.230	616	0.0225
0.115	2147	0.0289	0.507	1306	0.0561	0.035	738	0.0249
0.082	2042	0.0223	0.438	1422	0.0517	0.151	712	0.0361
-0.050	1826	0.0189	0.411	1581	0.0404	0.069	762	0.0204
0.133	1967	0.0317	0.137	1854	0.0304	0.171	766	0.0246
0.172	1767	0.0305	0.187	1572	0.0154	-0.023	605	0.0254
0.172	1767	0.0305	0.228	1645	0.0258	0.245	643	0.0225
0.396	1907	0.0345	0.196	1612	0.0461	0.061	697	0.0297
0.254	1910	0.0287	0.146	1712	0.0522	0.200	859	0.0249
-0.001	1142	0.0191	0.075	1650	0.0323	0.000	798	0.0257
0.274	1986	0.0284	0.239	1685	0.0423	-0.011	860	0.0236
0.149	1937	0.0261	0.149	1668	0.0326	0.128	680	0.0267
0.123	1965	0.0242	0.041	1681	0.0282	0.216	585	0.0265
0.302	1843	0.0241	0.465	1621	0.0394	0.135	661	0.0271
-0.014	1418	0.0244	0.013	1872	0.0226	0.059	549	0.0257
0.370	1953	0.0288	0.243	1445	0.0344	0.102	929	0.0192
0.220	1751	0.0326	0.058	1799	0.0338	-0.055	946	0.0217
0.001	2039	0.0271	0.060	1827	0.0281	0.146	636	0.0260
0.177	1852	0.0271	0.341	1469	0.0408	0.264	1019	0.0255
0.099	1936	0.0256	0.429	2039	0.0610	0.201	816	0.0232
0.115	1774	0.0258	0.171	2039	0.0418	0.159	905	0.0201
-0.007	1889	0.0193	0.472	1259	0.0441	0.138	879	0.0251
0.173	1280	0.0253	0.173	1727	0.0371	0.119	858	0.0246
0.143	1848	0.0297	0.182	1811	0.0297	0.295	675	0.0260
0.271	2130	0.0275				-0.110	857	0.0291
0.170	1738	0.0294				0.019	644	0.0241
0.090	1679	0.0183				-0.008	753	0.0248
-0.003	1977	0.0223				0.042	713	0.0274

Table 3

TS11			Lox-M			ZMI		
γ	$\sigma_{f.f(\gamma)}$	ς	γ	$\sigma_{f.f(\gamma)}$	ς	γ	$\sigma_{f.f(\gamma)}$	ς
0.170	1124	0.0258	0.220	1378	0.0185	0.125	1347	0.0162
0.131	1161	0.0203	0.220	1353	0.0199	0.034	1311	0.0165
0.185	1177	0.0179	0.246	1339	0.0197	0.226	1299	0.0284
0.221	1112	0.0257	0.331	1205	0.0233	0.165	1396	0.0255
0.145	1135	0.0155	0.125	1435	0.0172	0.261	1136	0.0213
0.033	1244	0.0145	0.270	1435	0.0222	0.201	1294	0.0198
0.018	1228	0.0129	0.222	1347	0.0176	0.110	1403	0.0176
0.178	838	0.0182	0.202	1405	0.0212	0.279	1230	0.0158
0.091	1202	0.0206	0.386	1387	0.0219	0.203	1329	0.0173
0.183	1050	0.0187	0.261	1429	0.0269	0.190	1329	0.0270
0.072	1127	0.0176	0.371	1439	0.0216	0.125	1350	0.0304
0.051	1133	0.0134	0.201	1294	0.0279	0.048	1371	0.0169
0.144	1167	0.0160	0.170	1385	0.0302	0.152	1396	0.0214
0.012	1261	0.0143	0.375	1496	0.0228	-0.012	1361	0.0145
0.015	1140	0.0174	0.209	1357	0.0227	0.073	1358	0.0240
0.035	1216	0.0203	0.174	1389	0.0337	0.129	1317	0.0293
0.152	1063	0.0222	0.205	1348	0.0262	0.045	1304	0.0156
0.023	1267	0.0113	0.314	1341	0.0324	0.033	1333	0.0215
0.331	1022	0.0235	0.368	1431	0.0235	0.255	1329	0.0263
0.115	1067	0.0192	0.179	1315	0.0346	0.145	1519	0.0244
0.030	1199	0.0188	0.385	1444	0.0284	0.147	1421	0.0203
0.108	1174	0.0174	0.255	1391	0.0224	0.073	1431	0.0215
0.050	1182	0.0181	0.339	1426	0.0219	0.015	1387	0.0171
0.040	1138	0.0135	0.143	1425	0.0174	0.117	1431	0.0167
0.172	1159	0.0229	0.143	1425	0.0166	0.235	1429	0.0272
0.224	1137	0.0175	0.350	1505	0.0205	0.226	1439	0.0261
0.020	1169	0.0169	0.217	1392	0.0245	0.204	1352	0.0201
0.110	1103	0.0143	0.218	1367	0.0294	0.138	1405	0.0199
0.106	1113	0.0161	0.204	1390	0.0268	-0.035	1366	0.0140
0.058	1002	0.0146	0.338	1428	0.0288	0.185	1341	0.0191

Table 4

NI207*			ZMI‡			ZMI_{Cl}		
γ	$\sigma_{f.f(\gamma)}$	ς	γ	$\sigma_{f.f(\gamma)}$	ς	γ	$\sigma_{f.f(\gamma)}$	ς
0.097	878	0.0324	0.392	912	0.0247	0.205	686	0.0145
0.256	890	0.0261	0.170	873	0.0129	0.237	537	0.0119
0.181	1055	0.0233	0.305	1112	0.0183	0.277	679	0.0186
0.146	990	0.0241	0.297	928	0.0150	0.154	570	0.0117
0.117	897	0.0224	0.187	1061	0.0150	0.474	1146	0.0205
0.150	972	0.0332	0.148	770	0.0206	0.368	1006	0.0180
0.199	794	0.0273	0.256	950	0.0221	0.289	1208	0.0182
0.232	841	0.0257	0.279	980	0.0235	0.249	662	0.0199
0.138	1070	0.0278	0.261	1072	0.0238	0.287	772	0.0181
0.321	934	0.0255	0.375	882	0.0211	0.320	674	0.0185
0.256	979	0.0358	0.303	973	0.0287	0.323	604	0.0194
0.278	1182	0.0205	0.283	1075	0.0234	0.240	978	0.0173
0.172	918	0.0253	0.232	890	0.0136	0.251	580	0.0170
0.352	908	0.0201	0.300	959	0.0295	0.189	948	0.0149
0.231	973	0.0296	0.176	819	0.0142	0.257	692	0.0174
0.199	701	0.0242	0.161	759	0.0207	0.210	622	0.0159
0.179	926	0.0184	0.165	971	0.0149	0.299	731	0.0192
0.171	741	0.0334	0.201	818	0.0178			
0.198	969	0.0225	0.225	840	0.0191			
0.191	996	0.0278	0.173	954	0.0166			
0.207	928	0.0286	0.276	1275	0.0165			
0.198	650	0.0289	0.296	1145	0.0185			
0.154	799	0.0254	0.233	1186	0.0181			
0.202	828	0.0384	0.357	995	0.0199			
0.141	692	0.0258	0.293	1213	0.0231			
0.184	816	0.0309	0.290	910	0.0175			
0.080	819	0.0227	0.297	1000	0.0209			
0.157	683	0.0270	0.260	729	0.0181			
0.151	688	0.0203	0.322	1102	0.0200			
0.302	652	0.0296	0.225	788	0.0247			

Table 5

	Number of tests	$\sigma_{f.t_{(\bar{\gamma})}}$ (MPa)	$F_{f.t}$ (N)	m_t	$\sigma_{0.t}$ (MPa)	Compliance (μm N^{-1})
NL101	30	870	57	4.8	940	1.6
NL207	30	750	57	7.8	810	1.4
NL207*	30	870	60	7.8	928	0.60
Hi-Ni	30	1800	120	7.9	1930	1.6
Hi-Ni-S	26	1600	82	9.0	1730	1.3
TS	100	1300	100	17	1380	0.90
TS11	30	1100	87	15	1180	1.6
Lox-M	30	1400	95	28	1420	0.80
ZMI	30	1350	110	23	1390	1.2
ZMI‡	28	960	57	8.1	1020	0.68
ZMI_{Cl}	18	770	37	4.4	840	1.3
AM	30	810	60	6.2	870	1.1

Table 6

	$\bar{\gamma}$ (%)	Me(γ) (%)	γ_{min} / γ_{max} (%)	m_γ	γ_0 (%)	$\bar{\varsigma}$ (N)	Me(ς) (N)	m_ς	ς_0 (N)
NL101	15 ± 13	14.3	-13 / 58	1.50	32.9*	0.0285	0.0262	5.39	0.0311
NL207	10 ± 10	11.1	-11 / 29	2.44	28.9*	0.0268	0.0259	6.86	0.0273
NL207*	20 ± 6.0	18.7	8.0 / 35	1.84	14.3*	0.0249	0.0250	8.70	0.0261
Hi-Ni	14 ± 12	14.3	-6.0 / 40	2.00	27.3*	0.0259	0.0260	6.93	0.0274
Hi-Ni-S	25 ± 16	21.2	1.3 / 53	1.36	29.0	0.0406	0.0399	3.53	0.0443
TS	16 ± 11.2	14.3	1.0 / 44	1.48	22.8	0.0099	0.0089	4.29	0.0097
TS11	10 ± 8.5	10.7	1.2 / 33	1.33	11.8	0.0179	0.0175	5.96	0.0186
Lox-M	25 ± 8.1	22.1	12.5 / 39	1.38	15.6*	0.0240	0.0228	5.84	0.0243
ZMI	14 ± 8.5	14.1	-3.5 / 28	2.29	23.6*	0.0211	0.0202	5.29	0.0216
ZMI‡	26 ± 6.5	26.9	14.8 / 39	1.49	13.6*	0.0198	0.0195	5.72	0.0208
ZMI_{Cl}	27 ± 8.0	25.7	15.4 / 47	1.86	16.6*	0.0169	0.0177	7.22	0.0163
AM	13 ± 11	13.1	-5.0 / 46	2.14	26.3*	0.0180	0.0171	5.54	0.0195

Table 7

NL207	TS	TS	TS11	Lox-M	Hi Ni	Hi Ni
700 MPa	700 MPa	500 MPa	700 MPa	700 MPa	1000 MPa	1500 MPa
650 °C	550 °C	650 °C	650 °C	650 °C	500 °C	500 °C
1198	46500	6783	4941	1985	2612	56
1336	57861	24263	8453	2441	13438	60
2377	92667	25281	10639	2673	14052	86
3491	189835	26858	13712	3261	16195	86
3654	229358	32539	15140	8362	16386	1148
5318	232633	35879	15878	9709	29241	1300
7546	240524	53981	17196	9955	31008	2081
9975	246014	60038	17303	10775	33905	3146
13980	265345	64396	17381	16168	33957	3453
25155	272211	69012	18772	17066	34137	3866
28068	306542	73977	19621	17324	39518	4261
31732	356840	77876	20862	18649	50205	5369
42121	377509	82018	23250	18763	52700	6803
57095	386300	85795	24726	19447	56072	7240
76123	414748	87669	25074	19773	71298	11420
80393	486407	90388	25194	20339	74099	23900
91866	435313	94951	26380	21326	94451	25041
102445	509817	105047	26685	22750	100728	29709
104586	543303	111772	30591	22817	114539	31223
113737	556292	114190	32430	28079	144820	34023
124731	583611	127467	35027	28897	153422	34148
133002	648384	137948	35537	28910	182008	40071
146905	708140	140008	37545	29599	196280	40728
168832	794509	158797	40446	36163	202380	44588
176073	820232	160676	41575	36565	225628	48126
268278	864154	169464	43143	37741	278471	52695
338775	877336	196330	49534	41079	288711	89101
348401	1070683	267717	56644	41216	448951	95798
678431	1165121	501459	60575	64163	536286	109083
809030	2456843		158326	104561	647954	
					1345475	

Table8

Fiber	Condition	$m_{df.t}$	t_0 (s)	Reference
NL207	700 MPa 650 °C	0.67	1.02×10^5	
Hi-Ni	1000 MPa 500 °C	0.91	1.50×10^5	[4]
Hi-Ni	1500 MPa 500°C	0.53	2.04×10^4	[4]
Hi-Ni	300MPa 900°C	0.45	2.66×10^5	[4]
Hi-Ni-S	1000 MPa 600 °C	0.78	2.06×10^5	[5]
TS	800 MPa 500 °C	1.46	5.88×10^5	
TS	600 MPa 550 °C	1.49	1.23×10^6	
TS	700 MPa 550 °C	1.44	6.05×10^5	
TS	800 MPa 550 °C	1.45	2.40×10^5	
TS	300 MPa 650 °C	1.44	1.32×10^6	
TS	500 MPa 650 °C	1.45	1.20×10^5	
TS	600 MPa 650 °C	1.44	4.93×10^4	
TS	700 MPa 650 °C	1.44	4.67×10^4	[6]
TS11	700 MPa 650 °C	1.83	3.50×10^4	
Lox-M	700 MPa 650 °C	1.30	2.66×10^4	
ZMI	700 MPa 650 °C	1.30	5.45×10^5	
ZMI‡	910 MPa 650°C	0.78	2.76×10^4	
ZMI‡	910 MPa 550°C	0.84	2.54×10^5	

Table 9

T (°C)	NL207		Hi-Ni		Hi-Ni-S		TS		TS11		Lox-M		ZMI	
	n_t	$A_t \times 10^{25}$ (s MPa$^{7.3}$)	n_t	$A_t \times 10^{26}$ (s MPa$^{8.4}$)	n_t	$A_t \times 10^{25}$ (s MPa$^{7.2}$)	n_t	$A_t \times 10^{19}$ (s MPa$^{5.0}$)	n	$A_t \times 10^{21}$ (s MPa$^{5.8}$)	n_t	$A_t \times 10^{19}$ (s MPa$^{4.9}$)	n_t	$A_t \times 10^{31}$ (s MPa$^{9.1}$)
350	-	-	-	-	-	-	-	600	-	-	-	-	-	-
400	-	-	-	-	-	-	-	200	-	-	-	1200	9.99	10000
450	-	1000	-	-	-	-	5.59	80	6.87	400	-	20	9.99	2000
500	6.92	400	8.45	10000	-	5700	4.81	38	5.34	80	4.67	80	11.35	300
550	7.66	40			-	-	5.26	17	4.68	30	5.49	20	9.24	60
600	-	30	-	400	7.25	250	4.84	6.0	5.48	20	5.17	1.8	8.37	6.0
650	7.05	15	-	-	-	-	4.34	0.80	6.81	4.0	4.25	0.40	8.71	0.70
700		-	-	32	-	20	-	-	-	-	-	-	-	-
750	7.63	1.0	-	-	-	-	5.29	0.50	-	2.0	-	0.10	8.39	0.30
800	-	-	8.34	4.0	7.24	2.7	-	-	-	-	-	-	-	-
850	7.25	0.30	-	-	-	-	-	0.20	-	1.0	-	0.10	9.16	0.12
900	-	-	-	0.70	-	-	-	-	-	-	-	-	-	-
550 (2)	-	60	-	-	-	-	-	-	-	-	-	-	-	14
650 (2)	7.23	8.0	-	-	-	-	-	-	-	-	-	-	7.28	0.70
750 (2)	-	0.80	-	-	-	-	-	-	-	-	-	-	-	-
$\overline{n_t}$	**7.3**		**8.4**		**7.2**		**5.0**		**5.8**		**4.9**		**9.1**	